National Library of Canada
Bibliothèque nationale du Canada

Canadian Theses Service
Service des thèses canadiennes

Ottawa, Canada
K1A 0N4

NOTICE

The quality of this microform is heavily dependent upon the quality of the original thesis submitted for microfilming. Every effort has been made to ensure the highest quality of reproduction possible.

If pages are missing, contact the university which granted the degree.

Some pages may have indistinct print especially if the original pages were typed with a poor typewriter ribbon or if the university sent us an inferior photocopy.

Previously copyrighted materials (journal articles, published tests, etc.) are not filmed.

Reproduction in full or in part of this microform is governed by the Canadian Copyright Act, R.S.C. 1970, c. C-30.

AVIS

La qualité de cette microforme dépend grandement de la qualité de la thèse soumise au microfilmage. Nous avons tout fait pour assurer une qualité supérieure de reproduction.

S'il manque des pages, veuillez communiquer avec l'université qui a conféré le grade.

La qualité d'impression de certaines pages peut laisser à désirer, surtout si les pages originales ont été dactylographiées à l'aide d'un ruban usé ou si l'université nous a fait parvenir une photocopie de qualité inférieure.

Les documents qui font déjà l'objet d'un droit d'auteur (articles de revue, tests publiés, etc.) ne sont pas microfilmés.

La reproduction, même partielle, de cette microforme est soumise à la Loi canadienne sur le droit d'auteur, SRC 1970, c. C-30.

NL-339 (r. 88/04)

Canada

THE UNIVERSITY OF ALBERTA

AN EXPERIMENTAL STUDY OF THE FLOW DEVELOPMENT REGION OF A BUOYANT JET

by

© ARBIND P. MAINALI

A THESIS

SUBMITTED TO THE FACULTY OF GRADUATE STUDIES AND RESEARCH

IN PARTIAL FULFILMENT OF THE REQUIREMENTS FOR THE DEGREE

OF MASTER OF SCIENCE

IN

CIVIL ENGINEERING

EDMONTON, ALBERTA

FALL, 1987

Permission has been granted to the National Library of Canada to microfilm this thesis and to lend or sell copies of the film.

The author (copyright owner) has reserved other publication rights, and neither the thesis nor extensive extracts from it may be printed or otherwise reproduced without his/her written permission.

L'autorisation a été accordée à la Bibliothèque nationale du Canada de microfilmer cette thèse et de prêter ou de vendre des exemplaires du film.

L'auteur (titulaire du droit d'auteur) se réserve les autres droits de publication; ni la thèse ni de longs extraits de celle-ci ne doivent être imprimés ou autrement reproduits sans son autorisation écrite.

ISBN 0-315-41184-8

THE UNIVERSITY OF ALBERTA

RELEASE FORM

NAME OF AUTHOR ARBIND P. MAINALI

TITLE OF THESIS AN EXPERIMENTAL STUDY OF THE FLOW DEVELOPMENT REGION OF A BUOYANT JET

DEGREE FOR WHICH THESIS WAS PRESENTED MASTER OF SCIENCE

YEAR THIS DEGREE GRANTED FALL, 1987

Permission is hereby granted to THE UNIVERSITY OF ALBERTA LIBRARY to reproduce single copies of this thesis and to lend or sell such copies for private, scholarly or scientific research purposes only.

The author reserves other publication rights, and neither the thesis nor extensive extracts from it may be printed or otherwise reproduced without the author's written permission.

(SIGNED) Arbind Mainali.....

PERMANENT ADDRESS:

Balaju, Chakrapath.....

Kathmandu.....

NEPAL.....

DATED .....8 June.....1987

THE UNIVERSITY OF ALBERTA

FACULTY OF GRADUATE STUDIES AND RESEARCH

The undersigned certify that they have read, and recommend to the Faculty of Graduate Studies and Research, for acceptance, a thesis entitled AN EXPERIMENTAL STUDY OF THE FLOW DEVELOPMENT REGION OF A BUOYANT JET submitted by ARBIND P. MAINALI in partial fulfilment of the requirements for the degree of MASTER OF SCIENCE in CIVIL ENGINEERING.

.....

Supervisor

.....

.....

Date 15 June 87

ABSTRACT

The flow development region of a buoyant jet has received very little attention both in terms of experimental as well as analytical endeavours. Since most of the practical problems of buoyant jets deal mainly with the established flow region, most of the research efforts in this field have dealt with this region alone.

This study attempts to analyse the axial velocity in the flow development region and also determine its length in the low Froude number range. Measurements of the velocity in this study have been made using the Hydrogen bubble technique. A Bernoulli-type analysis has been presented for the plane as well as the axisymmetric case and an attempt has been made to predict the length of the potential core based on the velocity. Together with this, the problem of inflow often associated with low Froude number buoyant jets has been discussed along with some measurements. This is followed by an account of the limitations of this study.

ACKNOWLEDGEMENTS

The author would like to sincerely thank Dr. N. Rajaratnam for his enthusiastic support and guidance throughout the course of this study.

The author greatly appreciates the help given by S. Lovell and L. Flint-Petersen in the construction and maintenance of the experimental set up. The assistance of R. Gitzel and D. Lathe with the Hydrogen bubble apparatus is also appreciated.

The financial support for this study was provided by the Natural Sciences and Engineering Research Council by means of grants to Dr. N Rajaratnam. This support is gratefully acknowledged.

Table of Contents

Chapter Page

1. INTRODUCTION 1

1.1 General Discussion 1

1.2 Jets, Plumes and Buoyant Jets 2

1.2.1 Turbulent Jets 2

1.2.2 Plumes 5

1.2.3 Buoyant Jets 8

1.3 Flow Development Region 11

1.4 Inflow Into Outfalls 13

2. LITERATURE REVIEW 15

2.1 Mechanics of Buoyant Jet Diffusion 15

2.2 Fully Developed Flow 18

2.2.1 Turbulent Jets 18

2.2.1.1 Turbulence Characteristics 19

2.2.2 Buoyant Jets and Plumes 20

2.3 Zone of Flow Establishment 22

2.4 Inflow Study 23

2.5 Study Objective 25

2.5.1 Flow Visualisation 26

2.5.2 Flow Measurements 26

3. EXPERIMENTAL INVESTIGATION 27

3.1 Introduction 27

3.2 Experimental Set-up 27

3.2.1 Jet Tank 27

3.2.2 Constant Head Arrangement 28

3.2.3 Rotameter 28
3.2.4 Hot Water Arrangement 31
3.2.5 Temperature Measurement 32
3.2.6 Nozzle and Gate Arrangement 32
3.2.7 Photographic Equipment 32
3.2.8 Dye Injection 35
3.3 VELOCITY MEASUREMENT 35
3.3.1 Laser Doppler Anemometry 35
3.3.2 Hydrogen Bubble Method 36
3.3.2.1 General 36
3.3.2.2 Velocity Calculation 38
3.3.3 Hydrogen Bubble Set-up 39
3.3.3.1 Operation 39
3.3.3.2 Pulsing Unit 42
3.3.4 Advantages and Limitations 42
3.3.4.1 Advantages 42
3.3.4.2 Limitations 43
3.4 EXPERIMENTAL PROCEDURE 43
3.4.1 Flow Visualisation 43
3.4.1.1 Inflow Study 45
3.4.2 Buoyant Jet Experiments 45
4. ANALYSIS OF EXPERIMENTAL RESULTS 49
4.1 General Equations 49
4.1.1 Potential Core 52
4.2 Inflow Mechanism 54
4.3 Effective Diameter 55

4.4 Velocity Field 56
4.5 Potential Core 57
4.5.1 Length 57
4.5.2 Maximum Velocity 70
4.6 Results of Inflow 70
5. CONCLUSIONS AND RECOMMENDATION 78
5.1 Conclusions 78
5.2 Limitations of the Study 80
5.3 Recommendation for Future Work 81
References 82
6. APPENDIX A 85
6.1 Flow Development Region of a Plane Turbulent Buoyant Jet 85
6.1.1 Introduction 85
6.1.2 Analysis 85
6.1.2.1 Potential Core 86
7. APPENDIX B 91
8. APPENDIX C 100

List of Tables

Table		Page
3.1	Table of Rotameter Specifications	31
3.2	The Relevent Parameters for the Experiments	48
4.1	Results of Inflow Study	55
4.2	Measured Velocity (cm/s)	58
4.3	Summary of Corrected Velocity, Diameter and Froude Number	59
4.4	Summary of F_o', U_o/V_o and d/D	60
8.1	Summary of the LDA Velocity Measurements	100

List of Figures

Figure		Page
1.1	Regions of Flow in a Buoyant Jet	12
2.1	Hypothetical Instantaneous Picture of a Plume	17
2.2	Schematic Diagram Explaining the Production of Large Vortices in a Plume	17
3.1	Exerimental Set-up	29
3.2	Schematics of the LDA System (after Steffler *et al.*, 1985)	37
3.3	Schematics of the Hydrogen Bubble Apparatus	40
4.1	Definition Sketch of the Potential Core	51
4.2	(a-y) Variation of u_m/U_o With x/d for Buoyant Jets	61
4.3	Variation of L/d with F_o	71
4.4	Axial Variation of U_m/U_o with F_o	72
4.5	Variation of d/D With F_o'	74
4.6	Variation of F_o With F_o'	76
4.7	Variation of U_o/V_o With F_o'	77
5.1	Potential Core Determination of a Buoyant Jet	79
6.1	F_o vs the Length of the Potential Core for a Plane Plume	90
7.1	(a-y) Graphical Estimation of the Nozzle Velocity (cm/s)	91
8.1	(a-b) u_m/U_o vs x/D for a Buoyant Jet for 2.5 cm Nozzle	101

List of Plates

Plate		Page
3.1	Jet Tank	30
3.2	Nozzle Used in the Experiment- 5cm dia.	33
3.3	The Potential Core and the Shear Layer Visualisation by Dye Injection	34
3.4	The Hydrogen Bubble Apparatus	41
3.5	Typical Hydrogen Bubble Lines F_o= 0.86	44
3.6	Flow Visualisation of a Buoyant Jet Showing Ring Vortex Structure	46

List of Symbols

b	velocity half width	L
b_c	pollutant half width	L
$b_{\hat{c}}$	pollutant half width due to buoyancy	L
b_o	outlet half width of a plane jet	L
B'	specific buoyancy flux	L^4/T^3
B	non dimensional parameter	-
$\hat{c}$	$g\Delta\rho$ (weight deficiency)	$M/(LT)^2$
c	pollutant concentration	M/L^3
d	corrected diameter of the nozzle	L
D	diameter of the nozzle	L
F_o	corrected densimetric Froude number at the nozzle	-
F_{or}	densimetric Froude number at the nozzle based on the radius	-
F_o'	full flow densimetric Froude number at the nozzle	-
g	gravitational acceleration	L/T^2
H	depth of penetration of inflow into the nozzle	L
L	length of the potential core	L
Q	discharge through the nozzle	L^3/T
r_o	radius of the nozzle	L
r	radial coordinate	L

T_a	ambient temp. in the tank	-
T_p	temperature of the plume at the nozzle	-
T'	temperature fluctuations	-
u_m	centreline mean velocity in the plume	L/T
U_m	velocity at the end of the potential core	L/T
U_o	corrected velocity at the nozzle	L/T
u'	local velocity fluctuations from mean in the axial direction	L/T
V_o	full flow velocity at the nozzle, equal to $Q/(\pi D^2/4)$	L/T
x	longitudinal coordinate	L
y	lateral coordinate	L
a_e	entrainment coefficient	-
ϵ	eddy diffusivity	L^2/T
κ	turbulent kinetic energy per unit mass	$(L/T)^2$
ν	kinematic viscosity	L^2/T
ρ	mass density at a point	M/L^3
ρ_a	mass density of the ambient fluid	M/L^3
ρ_o	mass density at the nozzle	M/L^3
$\Delta\rho_o$	mass density defect at the nozzle between the ambient and the plume	M/L^3
τ	turbulent shear stress	M/LT^2

1. INTRODUCTION

1.1 General Discussion

A buoyant jet discharging vertically into a stagnant uniform ambient is a special class of flow often associated with many environmental pollution problems. When waste discharges from industry, agriculture or domestic sources are released either into the hydrosphere or the atmosphere, they often come out as jets or plumes. These types of flows have an inbuilt mechanism for entraining large quantities of the surrounding ambient fluid which results in significant initial dilution of the effluent.

Several examples can be found in waste disposal methods where this mechanism has been used effectively. Outfalls that discharge sewage into the ocean through multi-port diffusers are typical examples. The sewage being less dense than the surrounding saline ambient, rises as a buoyant jet entraining the salt water and gets diluted in this process by turbulent mixing. A very similar case is that of a plume of waste gases coming out from a chimney stack which eventually mixes with the surrounding air and gets diluted. In both these cases after entering the environment, the diffusion and the dilution of these wastes is primarily dependent on the turbulence characteristics and the mean velocity of these jets and plumes.

Before going into any special class of jet diffusion it is necessary at this point to take a brief look at the

different forms of waste discharges. Basically these flows can be classified into three distinct categories based on the initial fluxes of momentum and buoyancy.

1.2 Jets, Plumes and Buoyant Jets

1.2.1 Turbulent Jets

When a jet is issuing from a nozzle without any buoyancy and is purely momentum-dominated, it is termed a jet. Depending on the geometry of the orifice , it could be a plane or axisymmetric jet. Extensive studies have been done on plane as well as axisymmetric jets (Rajaratnam, 1976). The analysis of jets involves the solution of the time-averaged Reynolds equations and the continuity equation.

Let the axial direction be x with u as the corresponding time averaged velocity and let r be the transverse direction with v being the corresponding time averaged velocity. After performing an order of magnitude analysis, neglecting laminar shear and using slender flow approximations as in the case of boundary layer analysis, the Reynolds equations for an axisymmetric jet can be reduced to

$$u \frac{\partial u}{\partial x} + v \frac{\partial u}{\partial r} = - \frac{1}{\rho} \frac{dp}{dx} + \frac{1}{\rho r} \frac{\partial r\tau}{\partial r} \qquad [1.1]$$

where p = the pressure outside the jet

τ = the turbulent shear stress

The continuity equation is written as

$$\frac{\partial ru}{\partial x} + \frac{\partial rv}{\partial r} = 0 \qquad [1.2]$$

On integration, Eq. 1.1 becomes the integral momentum equation and is written as

$$\frac{d}{dx} \int_0^\infty 2\pi r dr \rho u^2 = 0 \qquad [1.3]$$

This states that the momentum flux in the axial direction is conserved.

The integration of the continuity equation gives

$$\frac{d}{dx} \int_0^\infty ru \, dr = - Б \, v_e \qquad [1.4]$$

where Б is the nominal outer boundary usually taken where the velocity is reduced to 1% of the velocity on the axis of the jet and v_e is the entrainment velocity.

Following Taylor's hypothesis (Taylor, 1958), v_e can be written as

$$-v_e = a_e \, u_m \qquad [1.5]$$

where a_e is the entrainment coefficient which has a generally accepted value of 0.028 for axisymmetric jets.

The solution to the jet problem by the integral method involves first the determination of the velocity and the length scales. This is achieved using the conditions of the similarity of the velocity profiles and the solution of the integral Reynolds and the continuity equations. For circular turbulent jets, similarity analysis gives

$$u_m \propto 1/x \quad \text{and}$$
$$b \propto x$$

where u_m and b are respectively the velocity and length scales. This indicates that the centreline velocity is constantly decaying and that the jet spreads linearly.

Experimental evidence (Rajaratnam, 1976) indicates that the normalised velocity and the pollutant concentration profiles are described by Gaussian functions and can be written as

$$\frac{u}{u_m} = f(\eta) = \exp(-0.693\eta^2) \qquad [1.6]$$

and

$$\frac{c}{c_m} = \exp(-0.693(1/k^2)\eta^2) \qquad [1.7]$$

where $\eta = r/b$ and k is a constant equal to about 1.16 defined by $b_c = kb$. For the velocity scale the following equation can be used (Rajaratnam, 1976)

$$\frac{u_m}{u_o} = 6.3/(x/d) \qquad [1.8]$$

With the help of the experimental results the velocity half width can be written as

$$b = 0.1\ x \qquad [1.9]$$

1.2.2 Plumes

Plumes appear more frequently in problems associated with the environment than the ordinary momentum jets. Plumes are distinctly different from jets or even buoyant jets (to be discussed later) in that they are completely buoyancy-driven. Their main source of kinetic energy and momentum flux is the buoyancy.

The analysis in this case is very similar to the one presented for an ordinary jet except that here the buoyancy conservation equation becomes very important. Due to the absence of the initial momentum, the analysis is simpler and the flow variables are now dependent mainly on the buoyancy flux.

The fundamental equations for this case are slightly different. Using the slender flow and the Boussinesq approximations, the momentum equations reduce to

$$u \frac{\partial u}{\partial x} + v \frac{\partial u}{\partial r} = \frac{1}{\rho_a} \frac{1}{r} \frac{\partial r\tau}{\partial r} + \frac{g\Delta\rho}{\rho_a} \qquad [1.10]$$

Similarly, the conservation equation for the density defect reduces to

$$u \frac{\partial \hat{c}}{\partial x} + v \frac{\partial \hat{c}}{\partial r} = \frac{1}{r} \frac{\partial}{\partial r} \left(r\epsilon \frac{\partial \hat{c}}{\partial r} \right) \qquad [1.11]$$

where $\hat{c} = g\Delta\rho$

$\Delta\rho = \rho_a - \rho$

g = the acceleration due to gravity

ρ = the fluid density at any point in the plume

ρ_a = the ambient density

ϵ = eddy diffusivity

The integration of the momentum equation gives

$$\frac{d}{dx} \int_0^\infty \rho u^2 r \, dr = \int_0^\infty \hat{c} r \, dr \qquad [1.12]$$

which indicates that the rate of change of the momentum flux in the plume with respect to the axial distance is equal to the buoyant force per unit (axial) length of the plume.

The integral buoyancy conservation equation

$$\frac{d}{dx} \int_0^\infty ru\hat{c} \, dr = 0 \qquad [1.13]$$

shows that the flux of the density defect is conserved in the axial direction. Experimental results (Rouse *et al.*, 1952) indicate that the normalised velocity and density deficiency profiles are self similar and the exponential function describes these profiles satisfactorily. For

practical purposes (Rajaratnam, 1984)

$$\frac{u}{u_m} = f(\eta) = \exp(-0.693\eta^2) \qquad [1.14]$$

$$\frac{\hat{c}}{\hat{c}_m} = \exp(-0.693(1/k^2)\eta^2) \qquad [1.15]$$

The following expressions describe the variation of the velocity, length and density defect scales

$$u_m \propto \frac{1}{x^{1/3}}$$

$$b \propto x$$

$$\hat{c}_m \propto \frac{1}{x^{5/3}} \qquad [1.16]$$

It can be seen that the velocity scale for a plume decays more slowly than in the case of a jet. From the results of Rouse *et al*. we find

$$b = 0.085\ x \qquad [1.17]$$

and

$$b_{\hat{c}} = 0.0988\ x \qquad [1.18]$$

where $b_{\hat{c}}$ is the buoyancy half width and the entrainment

coefficient a_e = 0.047 (Rajaratnam, 1984). This is much larger than that for a jet which is about 0.028. The final equations for the velocity and density defect scales can be written as (Rajaratnam, 1984)

$$\frac{U_m}{U_o} = \frac{6.35}{F_{or}^{2/3}} \frac{1}{(x/r_o)^{1/3}} \qquad [1.19]$$

$$\frac{\Delta\rho_m}{\Delta\rho_o} = \frac{19.73\ F_{or}^{2/3}}{(x/r_o)^{5/3}} \qquad [1.20]$$

where F_{or} is the nozzle-radius-based densimetric Froude number written as,

$$F_{or} = \frac{U_o}{\sqrt{g\ (\Delta\rho_o/\rho_a)\ r_o}}$$

where U_o = the velocity at the efflux port of radius r_o, $\Delta\rho_o$ = $\rho_a - \rho_o$ and ρ_o = the density of the effluent.

1.2.3 Buoyant Jets

Buoyant Jets probably occur more commonly than either jets or plumes. Sewage discharges issuing from diffusers in the ocean are generally buoyant jets. The slightly lower density of the sewage as compared to the saline ambient provides the density defect and hence the buoyancy-generated additional momentum flux. In these types of flows, in order

to prevent the saline intrusion into the outfall tunnels, certain initial momentum is provided. As the buoyant jet rises, the buoyancy-generated momentum increases and eventually dominates the initial momentum flux and the buoyant jet behaves more like a plume than a jet.

The analysis of a buoyant jet is somewhat more involved than that of a pure plume or jet. The presence of the initial momentum requires the formulation of an extra equation. An integral energy equation can be obtained by multiplying the momentum equation 1.10 by u and integrating

$$\frac{d}{dx}\int_0^\infty \rho_a \frac{u^3 r\, dr}{2} = -\int_0^\infty r\tau \frac{\partial u}{\partial r}\, dr + \int_0^\infty \hat{c}\, ur\, dr \qquad [1.21]$$

This equation indicates that the flux of the kinetic energy in the buoyant jet is increased by the work done by buoyancy and reduced by turbulence production.

Assuming similarity profiles, the above integral equations can be analysed. Assuming that the velocity half width of the pollutant is the same as that for a plume

$$b_c = kb \qquad [1.22]$$

where k is a constant equal to 1.16 and

$$b = k_2 x \qquad [1.23]$$

where k_2 is another constant equal to 0.097, the centreline velocity can be expressed nondimensionally as (Rajaratnam, 1984):

$$\frac{u_m}{U_o} = \left[\frac{259}{F_{or}^2 \, (x/r_o)} + \frac{1786}{(x/r_o)^3} \right]^{1/3} \qquad [1.24]$$

The relation for the density defect is:

$$\frac{\Delta\rho_m}{\Delta\rho_o} = \frac{100}{\left[120/F_{or}^2 \, (x/r_o)^5 + 840 \, (x/r_o)^3 \right]^{1/3}} \qquad [1.25]$$

The Froude Number at any distance x is given as:

$$F_r = \left[20.74 + \frac{6.73 \, F_{or}^2}{(x/r_o)^3} \right]^{1/2} \qquad [1.26]$$

where numerical values have been used for k and k_2.

The entrainment coefficient, unlike that in jets or plumes, is not constant. The total entrainment coefficient can be evaluated as a sum of the jet entrainment component a_{ej} and the plume entrainment component. If k = 1.16 and k_2 = 0.097

$$a_e = a_{ej} + \frac{0.44}{\left[20.74 + 6.73 \, F_{or}^3/(x/r_o)^3 \right]} \qquad [1.27]$$

The above equation shows the entrainment coefficient as a function of the nozzle Froude Number as well as the axial distance from the nozzle.

In the discussion so far all the attention has been focussed on the axisymmetric jet flows. Similar treatment of plane jets, plane plumes and plane buoyant jets can be found in the literature (Rajaratnam, 1976; Rajaratnam, 1984; Kotsovinos, 1977). Since the object of this study was to concentrate on the flow development region of an axisymmetric buoyant jet, emphasis has been placed on the axisymmetric case.

1.3 Flow Development Region

So far we have considered jets, plumes and buoyant jets in the region away from the source where the flow is said to be fully-developed. Close to the source, for a length which is a few times the diameter of the source, the flow is said to be developing and this region is referred to as the Zone of Flow Establishment or ZFE (Fig. 1.1). For jets, the length of this zone is about 6D whereas for plumes it appears to be somewhat shorter. This region (ZFE) has a central core where the flow is approximately irrotational and starts from the nozzle exit and extends up to a point where the surrounding shear layer penetrates the symmetric axis. This region is unique from the other regions in that it has two distinct zones. As the jet enters the stagnant ambient, due to the velocity discontinuity it encounters a shear stress starting from its outer boundary which gradually penetrates into the flow. This is the axisymmetric shear layer which becomes turbulent in most practical cases

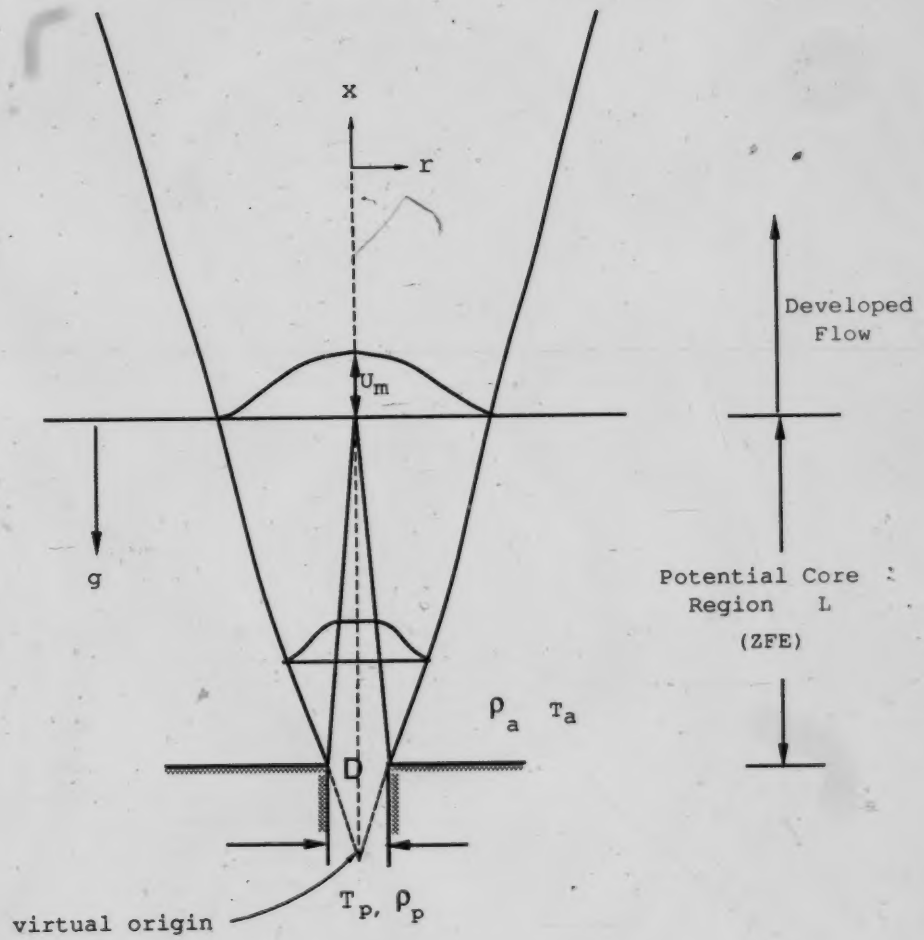

Figure 1.1 Regions of Flow in a Buoyant Jet

right from the nozzle. The inner core, which is constantly tapering, essentially remains undisturbed by the external mixing.

Since most of the important practical problems lie in the zone where the flow is fully developed, very little work has been done in this ZFE. Therefore our present knowledge of this region is limited. Furthermore, not only is the physics of the region intriguing but, also, the complexity involved in coming up with accurate measurements in this region is a real challenge.

An extensive account of the studies made on the shear layer for jets has been presented by Rajaratnam (1976). Experimental observations made on the annular shear layer of turbulent jets clearly show the similarity of the velocity profiles. However, the profiles are not similar in the potential core.

1.4 Inflow Into Outfalls

One of the main concerns in buoyant jets is the problem of inflow of ambient fluid into the source. Sea outfalls are generally preferred for the disposal of the effluents from the land. These outfalls terminate in some kind of multi port diffuser which efficiently performs the initial dilution of the contaminants. These diffusers lie in such areas that the initially diluted waste discharges are swept away by ocean currents and diluted further. However, these diffusers do not always function as well as they were

intended to. Over the years these diffusers have been found to be back-filled with saline water starting from the farthest port making the system more and more inefficient. Because of the nature of the contaminants and the position of these diffusers far out into the ocean bed, it is difficult to completely observe and thus understand the mechanism involved in this problem.

Model studies performed by Wilkinson (1984) and Charlton (1982) and results of the recent studies to be discussed later seem to indicate that this problem is more prevelant when the initial momentum is small. The general belief, based on intuition, is that the exit densimetric Froude Number should be larger than unity to avoid saline intrusion (Brooks, 1970).

A similar problem is also faced in chimneys discharging hot waste gases into the atmosphere. The cold flow into the chimney has a tendency to form cold patches on the chimney wall. This has the effect of condensing vapours on to the cold wall. This moisture reacts with the exhaust gases to form corrosive acidic substances. Studies performed by Jörg and Scorer (1967) have pointed to the importance of the boundary layer at exit in addition to the densimetric Froude number at the exit. Hence, with this understanding of inflow, one of the objectives of the present study was also to make some observations of this problem using dye injection techniques and see the effect of exit densimetric Froude number on the intrusion of the ambient fluid.

2. LITERATURE REVIEW

2.1 Mechanics of Buoyant Jet Diffusion

The mechanics of Buoyant jet diffusion can be described starting from the point of discharge at the nozzle, the passage through the instabilities in the shear layer and the flow in the potential core, the shedding of large scale vortices and finally the fully developed turbulent flow.

The phenomenon of jet development is still a controversial topic. The mechanism of entrainment and the coherent structures has generated tremendous interest lately. What appears to be a random chaotic fluid motion has a very coherent structure present in it.

In 1957 Wehrman and Willie (Rodi, 1982) observed ring and helical vortices in turbulent jets and also that the frequency of the ring vortex production was proportional to the jet nozzle velocity. These vortices have their origin in the shear layer. Freymuth (1966), investigating the stability of shear layers formed at jet outlets, indicated the existence of axisymmetric and helical modes of wave growth on the shear layer. When a jet advances, the velocity differences between the inside and the outside of the jets, combined with the instabilities, have the effect of producing a rolling surface. The ambient fluid now experiences a velocity field and rolls on with the jet fluid in a series of *jelly rolls*(Rodi,1982).

Kotsovinos(1977) explains the formation of the vortices in a jet involving buoyancy as follows:

> If the volume of the fluid V_{xy} in between the section xx and yy in a plume of configuration indicated in figure 2.1 is considered, the temperature decreases and the density increases on the plume axis as the distance from the nozzle is increased. Thus the centre of mass of the volume V_{xy} will be above the centre of the pressure forces. Here two forces will be acting on the mass enclosed in this control volume V_{xy} - the gravitational force (G) acting at the centre of mass and the archimedean force (A) acting at the centre of the pressure force. Any slight disturbance could result in the configuration shown in figure 2.2 where the moment between the above two forces tends to overturn the volume V_{xy} and thus the inception of the large-scale vortices observed in a plume.

Kotsovinos further explains that the vortices in a plume, being larger than those in a jet, reach the central jet region earlier. This explains one of the reasons why the potential core is shorter in a plume. Furthermore, the larger structures of a plume also entrain a larger mass of the surrounding ambient fluid. This explains why the entrainment coefficient is larger in plumes, unlike the hypothesis postulated by Taylor(1958) and further developed by Morton(1959). This obviously explains why the jet width

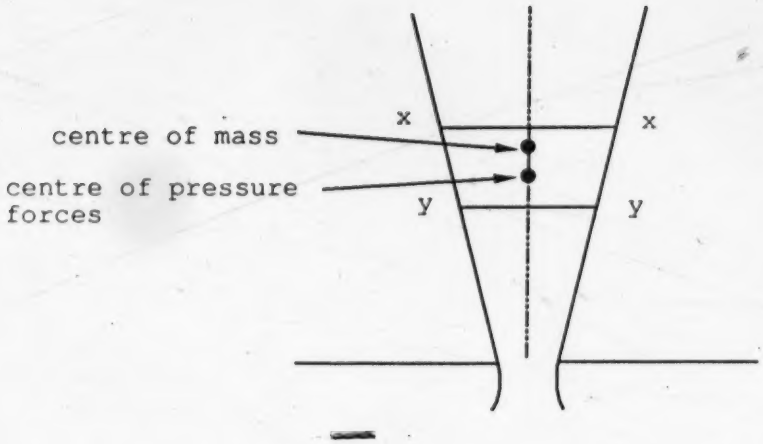

Figure 2.1 Hypothetical Instantaneous Picture of a Plume(after Kotsovinos, 1977)

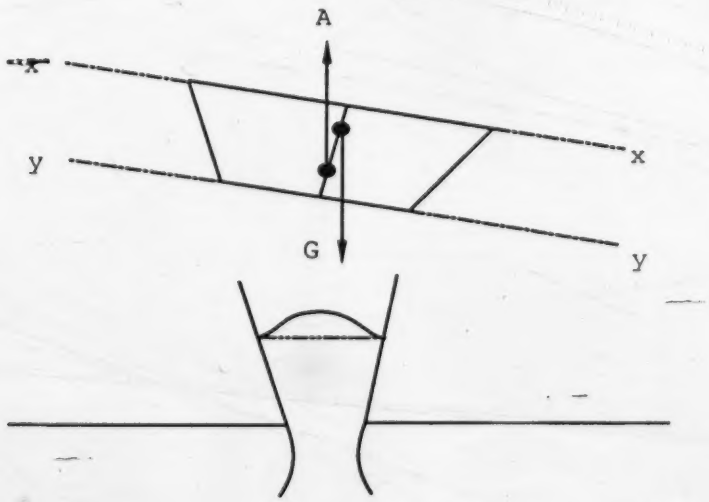

Figure 2.2 Schematic Diagram Explaining the Production of Large Vortices in a Plume (after Kotsovinos, 1977)

is greater in a jet involving buoyancy.

2.2 Fully Developed Flow

2.2.1 Turbulent Jets

The study of turbulent jets was first invstigated by Young in 1800 where he pointed out the lack of dependence of the included angle of the jet on the jet velocity. A fairly large volume of work can be found on turbulent jets. A brief outline of the experimental results as presented by Rajaratnam (1976) follows.

The above author cites Trupel (1915), Reichardt (1942), Corrsin (1946), Hinze and Zynen (1949), Albertson *et al.* (1950) who made the earlier investigations on axisymmetric turbulent jets. Each of the above investigations have presented their results of the velocity scales and the velocity half width. Following the Goertler-type solutions Reichardt observed

$$\frac{u_m}{U_o} = \frac{5.75}{x/d} \qquad [2.28]$$

Experimental results of Hinze and Zynen suggest

$$\frac{u_m}{U_o} = 6.39/\left(\frac{x}{d} + 0.6\right) \qquad [2.29]$$

where they observed that the virtual origin (Fig 1.1) was

located 0.6D behind the nozzle. Albertson *et al.* found that:

$$\frac{u_m}{U_o} = \frac{6.2}{x/d} \qquad [2.30]$$

In the case of the velocity half width b = kx ,Corrsin's data gave the value of k = 0.082. Abramovich suggested 0.097 on analysing Russian and German data. Albertson *et al.* suggested 0.0965 and Hinze and Zynen 0.094. Rajaratnam suggests 0.1 for all practical purposes.

2.2.1.1 Turbulence Characteristics

The problem with turbulence measurements has been the lack of reliable instruments for the measurement of the negative as well as the positive velocity. Before the Laser Doppler Anemometry (LDA) systems were available, hot wire and hot films were the only available velocity measuring instruments.

Wygnanski and Fiedler (1969) (see Rodi 1982), using hot- wire, found out that the turbulent stress equilibrium is reached only for x/d of 50 and above and the ratio $\sqrt{\overline{u'^2}}/u_m$ on the axis $\simeq$ 0.28 - 0.29. However, the pioneering study on buoyant jets was done by Kotsovinos (1977). His study was performed using the Laser Doppler Velocimetry on two dimensional jets and showed that at times flow in most jets could be reversed.

2.2.2 Buoyant Jets and Plumes

Several investigations can be found where studies on jets have extended to cases involving buoyancy. However, the volume of work done on buoyant jets and plumes is very little compared to studies done on non-buoyant jets. The reason, very clearly, is that the overlapping temperature and the velocity fields are very difficult to measure. Simultaneous measurement of the instantaneous temperature and the velocity fields requires sophisticated measuring and calibrating techniques as well as ingenuity in using these techniques for obtaining reliable results.

Apparently,one of the earlier investigation of buoyant plumes in a uniform environment was performed by Schmidt in 1941 (Rodi, 1982) as opposed to studies in jets that date as far back as 1800 performed by Young. Schmidt extended the mixing length theories and presented the results that show the decay of the centreline velocity is proportional to $x^{-1/3}$ and that of temperature proportional to $x^{-5/3}$. Results presented by Rouse *et al.* (1952) of measurements made on plumes above a gas burner can be reduced to:

$$u/u_m = \exp(-96r^2/x^2) \qquad [2.31]$$

for axial velocity profiles and

$$\Delta\rho/\Delta\rho_o = \exp(-71r^2/x^2) \qquad [2.32]$$

for temperature profiles which indicates the larger extent of temperature diffusion in the radial direction than momentum.

Further experiments performed by Nakagome and Hirata (1976) conclude, unlike Rouse *et al.*(1952), that the half width of the temperature distribution is smaller than the velocity distribution which indicates that the thermal energy diffusion in the radial direction is larger than momentum diffusion.

As far as the velocity decay in the axial direction is concerned, dimensional analysis gives

$$u_m = C\ (B'/x)^{1/3} \qquad [2.33]$$

where B' is the specific buoyancy flux $gQ\Delta\rho_o/\rho_o$. However, the suggested values of the constant C for plumes has a large range of 3.4 to 4.7. This demands a more careful study.

After the more sophisticated measurement techniques have become available, quite a few people have made measurements of turbulent velocity and temperature fluctuations. Measurements made by Nakagome and Hirata (1976), Kotsovinos(1977) and George *et al.*(1977) show the

relative velocity fluctuations $\sqrt{\overline{u'^2}}/u_m$ as 0.27 for axisymmetric plumes and 0.40 for plane plumes. The reason for this difference has not been determined yet.

As far as the buoyant jet is concerned, the pioneers were Morton *et al.* (1956) and Priestly and Ball (1955). They took the integrated form of the equations of motion and came up with the relationship of volume flux change. Morton *et al.* came up with the entrainment equation as introduced by Taylor, while Priestly and Ball came up with an entrainment function using the conservation of energy equation. However, the factor common to all these studies is that they were for the fully developed region.

2.3 Zone of Flow Establishment

Unlike the other regions, the potential core region has received very little attention. Only a handful of studies, numerical and experimental, have dealt with the flow in this region. Furthermore, studies in the buoyancy-dominated region are, apparently, non-existent.

Chen and Nikitopoulos(1979) approached the problem using the differential $\kappa - \epsilon - \overline{T}'^2$ model proposed by Chen and Rodi (1975) where κ is the turbulent kinetic energy per unit mass and ϵ is the eddy diffusivity. They calculated the lateral temperature, the velocity profile and the half width for turbulent buoyant jets in the flow development region for F_{or} ranging from 1 to 625. Their results predict the limiting length of the ZFE as 8D for jets and 7D for plumes.

They indicated a strong influence of initial turbulence level in the length of the zone of flow establishment and conclude that the axial Froude number at the end of the ZFE should be used as the initial condition for the equations describing the flow since only then does the decay of the axial velocity start.

Hirst(1972) also solved this problem using a numerical approach. He took the equations of mass, momentum and energy conservation and predicted the length of the zone of flow establishment, jet width, jet orientation and the centreline temperature in this zone. He used an entrainment function taking into account all the parameters that effect entrainment. For the non-buoyant region he shows a good agreement with the data from the study of Sami *et al.* (1966). Apparently, the study of Sami *et al.* proves to be the only extensive work in the ZFE. However, this study was for a non-buoyant air jet passed through a nozzle one foot in diameter. Mean flow and turbulence measurements were made in this study. One of the conclusions made in this study was that the large scale eddy was independent of the jet velocity.

2.4 Inflow Study

One of the main concerns in buoyant jets in the low Froude number range is the problem of inflow of the ambient fluid. This is a major problem in tunnelled ocean sewage outfalls where a saline wedge is formed if the discharge

through the riser is less than a certain critical discharge. Wilkinson(1984) simulated the tunnel-riser system in the lab and made measurements for purging saline wedges using discharge, the nozzle diameter and the riser lengths as the variables. His calculations show that a port Froude number of 7.8 is required to purge the saline wedge from the tunnel at *start-up*. With reference to Jörg and Scorer(1967) he states that inflow into the diffuser would be avoided if the outlet densimetric Froude number based on the diameter and the efflux velocity is greater than unity. Charlton (1982) in his model study of the Aberdeen sea outfall, points out the general accceptance of the critical Froude number requirement to be greater than unity for the prevention of an intrusive condition. Brooks(1970) intuitively uses a Froude number of unity for rounded port as a criteria for full flow.

Jörg and Scorer(1967) in their study of intrusion into smoke stack, suggest that the boundary layer near the exit is also important in determining intrusion along with the exit Froude number. The results from their set-up using salt water and plain water and the supplementary work with hot air for large Reynolds number seem to indicate that the intrusion was not dependent on the dimensions of the nozzle. They did find a critical exit velocity at which no intrusion would occur which was seen to be a property of the velocity profile near the tube wall. The critical velocity was given by the relation

$$\frac{Bg\nu}{V_{oc}^{3}} = \text{const.} \qquad [2.34]$$

where $B = \Delta\rho_o/\rho$

ν = kinematic viscosity of the plume fluid

V_{oc} = critical velocity at the nozzle

The constant for a fully developed turbulent velocity profile was 8×10^{-4}. It is apparent that if the velocity is increased, the inflow would stop but if the boundary layer can be made thinner without increasing the total mass or momentum flux, this would inhibit the inflow too.

Their study on depth of penetration, H, yielded the following relation for a fully established turbulent boundary layer on a smooth wall

$$\frac{Bg\nu}{(H^2 + 8)^3 V_o^3} = 10^{-6} \qquad [2.35]$$

2.5 Study Objective

At this stage our understanding of the flow development region of a buoyant turbulent jet is limited. Very few studies on the flow development region can be found. With this understanding in mind the objective of this study was to make investigations in two distinct areas.

2.5.1 Flow Visualisation

One of the main objectives of the study was to spend some time in the study of the physical behaviour of a buoyant jet in the region near the nozzle and in the potential core. This would be done by injecting dye and recording the observations on photographs. A preliminary study of the large scale vortex structures and their behaviour combined with the study of the intrusion problem was planned.

2.5.2 Flow Measurements

In order to measure the velocity field in the Flow Development Region it was planned to make measurements using the two velocity measurement facilities available at the T. Blench Hydraulics Laboratory, University of Alberta, namely the LDA and the Hydrogen Bubble method. The turbulence measurements would be measured by the LDA and the mean velocity compared with that measured using the Hydrogen Bubble Method.

3. EXPERIMENTAL INVESTIGATION

3.1 Introduction

The experimental set-up as well as the Hydrogen Bubble measuring system were assembled in the T. Blench Hydraulics Laboratory and the Civil Engineering Electronics Laboratory at the University of 'Alberta. The LDA system was also available in the Hydraulics Laboratory. All the experiments in this study were carried out in the T. Blench Hydraulics Laboratory.

The stagnant ambient in the tank was the regular city water supply and the buoyant jet was generated using the hot water available in the laboratory A detailed discussion of the experimental set up and the procedure is presented next.

3.2 Experimental Set-up

3.2.1 Jet Tank

The buoyant jet experiment was carried out in a square tank of side 1.22m and height of 1.22m. The side walls of the tank were made of 10 mm thick clear plexiglass, structurally supported by steel channels and angle sections welded together. Plate 3.1 gives a view of the tank. The base was a 6.5 mm aluminum plate with a 10 cm circular nozzle opening at the centre.

The discharge from a constant head tank was led through an 8 inch dia. tube and a bellmouth shaped reducer ending at the nozzle. At the top of the jet tank, overflow water was passed over the overflow weir into a channel 6.5 cm wide running all around the tank and finally emptied into the drain. An opening was also provided at the base of the tank for draining purpose. Fig. 3.1 gives a sketch of the set-up.

3.2.2 Constant Head Arrangement

The constant head arrangement consisted of a tank suspended from the ceiling which was fed by a 0.25 kW pump. This tank, in which a constant level was maintained, provided the flow for the jet. In order to maintain a steady discharge into the nozzle, the overflow line had to be kept at least partially flowing.

3.2.3 Rotameter

The discharge through the nozzle was measured with rotameters calibrated by volumetric measurement. To prevent non-uniform discharge through the nozzle, the rotameters were placed after the constant head tank (Fig. 3.1). The constant head arrangement also helped eliminate the non-uniformity in the flow.

Since the range of flow was from 0.2 Lpm to 30 Lpm, 3 different rotameters were connected in parallel so that any one or all of them could be used simultaneously. The

Figure 3.1 Experimental Set-up

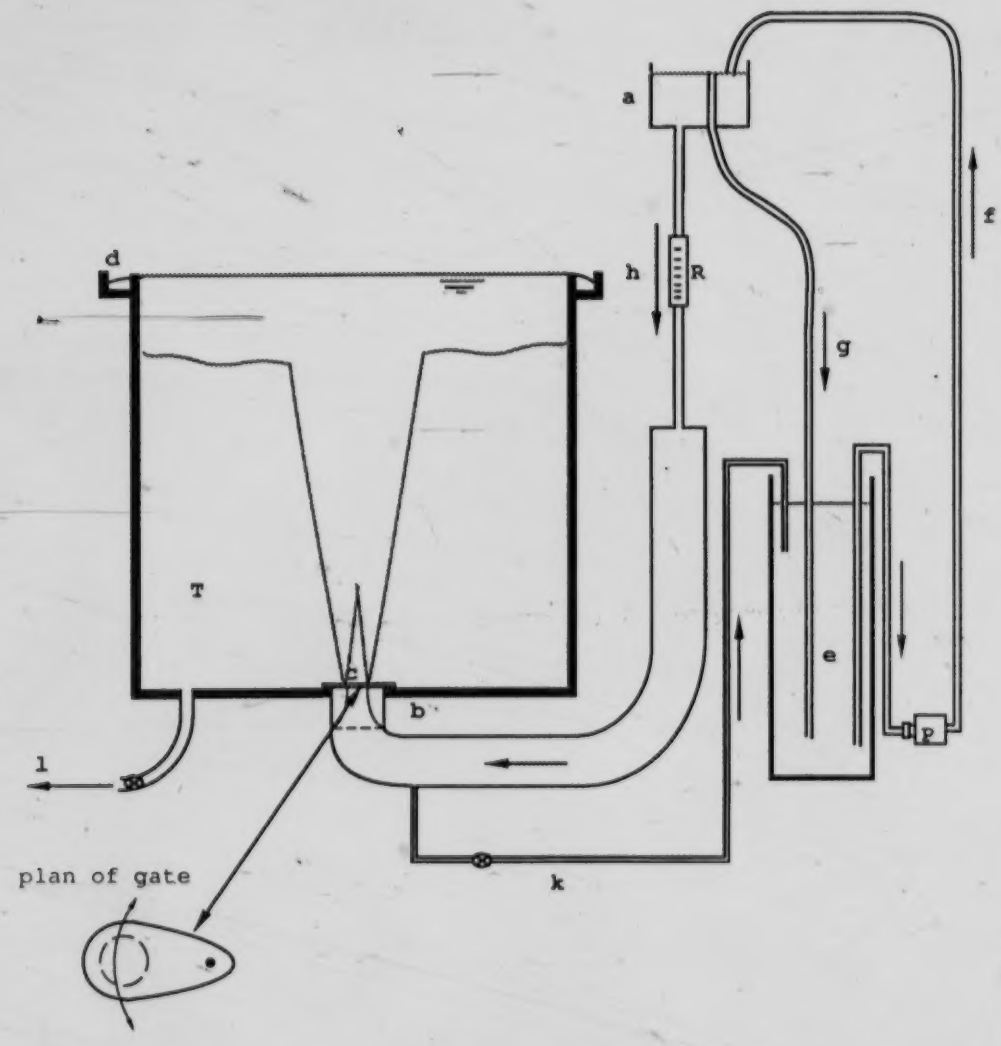

a = Constant head
b = Nozzle
c = Potential Core
d = Overflow Channel
e = Hot Water Tank
f = Hose to Constant Head
g = Over flow from Constant Head
h = Hose to Nozzle
k = Recirculation Hose
l = To Drain
T = Jet tank in text
P = Pump
R = Rotometer

Flow Direction

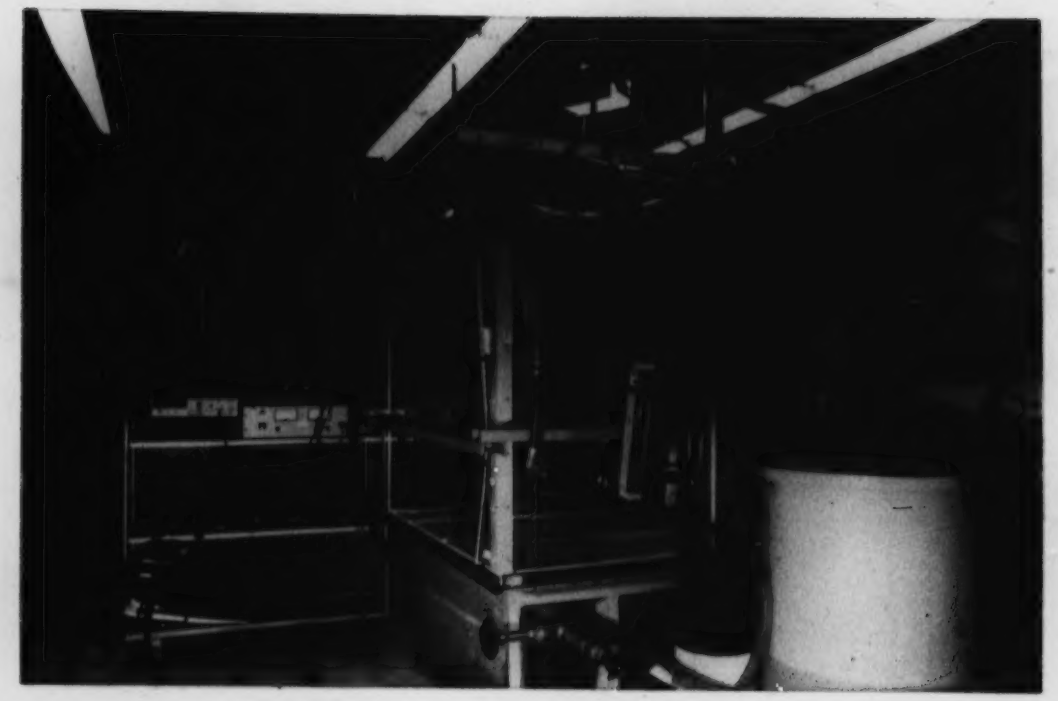

Plate 3.1 Jet Tank

specifications of the rotameters are as following:

Table 3.1 Table of Rotameter Specifications

Rotameter	Range	Unit
a	5.0 - 40.0	Lpm
b	0.6 - 3.4	Gpm
c	0.2 - 1.3	Lpm

3.2.4 Hot Water Arrangement

The warm water required for the buoyant jet was taken from a boiler and mixed with cold water to get the desired jet temperature in a separate tank of 0.22 m^3 capacity. Generally it was found that the temperature difference in the vicinity of 10 to 12 °C between the plume and the ambient fluid was ideal for obtaining good and sustained hydrogen bubble streaks. At higher temperature differences, instabilities in the plume tended to sweep the hydrogen bubble lines laterally making photographic records very difficult.

The mixed warm water was then circulated through the pump system, the constant head tank and the bypass from the nozzle (efahk, Fig. 3.1) keeping the nozzle gate closed until a uniform temperature was achieved. At this point the

bypass was closed and the nozzle opened. The required discharge then was controlled by a valve at the rotameter.

3.2.5 Temperature Measurement

Temperature measurements in this study were made using a Fluke 2180A and 51K/J Fluke RTD digital thermometers with respective accuracies of 1/10 °C and 1/100 °C. These thermometers were calibrated with measurements from a mercury thermometer. In order to maintain consistency, all the measurements for one run were made by one thermometer.

3.2.6 Nozzle and Gate Arrangement

Three different sizes of nozzles were used for this study. The original nozzle in the set-up was 10 cm dia. The 2.5 cm and the 5 cm diameter nozzles, bellmouth shaped at one end, were made by turning brass cylinders on a lathe (Plate 3.2). The external diameters were 10 cm so they fit in the 10 cm diameter nozzle in the tank. They were set in using silicon sealant which prevented leakage.

The gate was made with a 6.5 mm thick plate with an eccentric axle (Fig. 3.1). It was operated manually from outside the tank using strings.

3.2.7 Photographic Equipment

The photographs were taken using ASAHI PENTAX 35mm camera. It was found that due to the large depth of water in

Plate 3.2 Nozzle Used in the Experiment - 5cm dia.

Plate 3.3 The Potential Core and the Shear Layer Visualisation by Dye Injection

the tank, the external lighting was diffused and therefore, for high shutter speed a film speed of ASA 200 was convenient. A shutter speed of 1/250 and an aperture larger than 2.5 produced a satisfactory depth of field.

For lighting, three Color Tran arc lamps, each 650 watts, were used, with one projected from the top of the tank and two projected at an angle from the side.

3.2.8 Dye Injection

As a part of the study, dye injection was carried out in two ways. In one method Cochineal food color was mixed to the jet fluid and this colored the whole jet (plate 3.6). In the second method dye was injected at the nozzle exit from the two sides (plate 3.3) through 1.5 mm tubes feeding from an elevated dye jar. The dye had to be injected without any initial momentum.

3.3 VELOCITY MEASUREMENT

3.3.1 Laser Doppler Anemometry

Laser doppler anemometry (LDA) for turbulence measurement is probably the best method in this particular experiment, if it doesn't pose any difficulty in instrument deployment.

Because of the complex pattern of flow in the flow development region of the jet, an accurate measurement of

velocity was required. It was thought that the use of LDA would be the best method. The system available at the T. Blench Hydraulics Laboratory was a DANTEC LDA system (Fig. 3.2). A 4W Argon-Ion laser was used. The optical configuration was a two color, 3 beam type used in a back scatter differential doppler mode. The focal length used was 600 mm and the optics were rotated in such a way that the common and the blue beam were parallel to the bottom of the tank and the green converged down to the intersection of the beams. The traverse was a 3D traverse with a positioning accuracy of ±10 μm. Different types of seeding were used but the best result was obtained with aluminum powder. However, the data rate and the validation were very low. The problem was further amplified by the bending of the plexiglass side wall due to the hydrostatic load which created problems for the laser optics. This avenue had to be finally abandoned.

3.3.2 Hydrogen Bubble Method

3.3.2.1 General

This technique of velocity measurement is fairly old. Clutter, Smith and Brazier (1959) who pioneered the development of the technique to its present form indicate that this is an outcome of the method evolved by F. X. Wortman who passed current through a wire to release telerium in order to generate time lines.

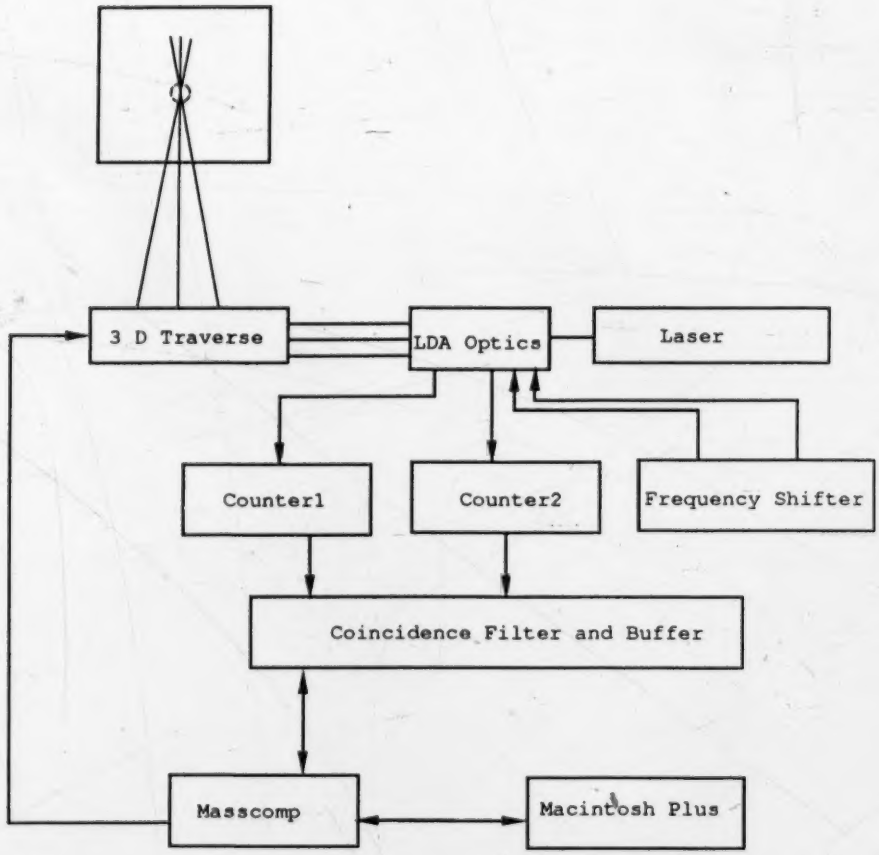

Figure 3.2 Schematics of the LDA System
(after Steffler *et al.* 1985)

This method is essentially an electrolysis method. High voltage is passed through a fine tungsten wire placed across the flow. The hydrogen bubbles produced at the wire are swept off by the flow. On subjecting the electrode to a pulsating square wave current, the bubbles build up and are swept off in continuous lines. If a constant frequency pulse is passed through the wire stretched normal to the flow, a fine screen of lines can be observed which can be measured to give the velocity of the moving fluid.

3.3.2.2 Velocity Calculation

The longitudinal velocity is given by the relation

$$u = \frac{\Delta x \; N}{S_f}$$

$$u = \frac{\Delta x}{S_f T} \qquad [3.36]$$

Δx is the spacing between two consecutive lines

S_f is the scale factor defined as the ratio of the average distance on the film between the two lines closest to the wire in the photograph to its actual distance in the water. This was determined by photographing a scaled grid in the water from a camera position fixed for the whole run.

N is the Number of pulses per second.

T is the time period of the pulses

3.3.3 Hydrogen Bubble Set-up

Fig. 3.3 gives a schematic of the hydrogen bubble apparatus. The set-up consists of the following:

Voltage source (Hewlett-Packard 0-600 V, 0-1.5 A)

Pulsing Unit

Counter timer unit (Fluke 1953A)

Frame for holding Wire and 0.6 mm tungsten wire

Tungsten-lamp

Camera

Grid

Traverse arrangement

The high voltage DC power supplier unit supplies the voltage to the tungsten wire through a solid state FET switch which is turned on/off by the pulse from the pulsing unit. The time period is recorded and displayed on the digital display of the counter timer unit. The water in the tank is electrolysed at the tungsten wire electrode and the camera takes photographs of the lines of the hydrogen bubbles.

3.3.3.1 Operation

Unlike the LDA system, the operation of the hydrogen bubble apparatus posed very little problem. The set-up was started up by first turning the pulsing unit on. The counter timer unit was then turned on. Finally the voltage unit was turned on.

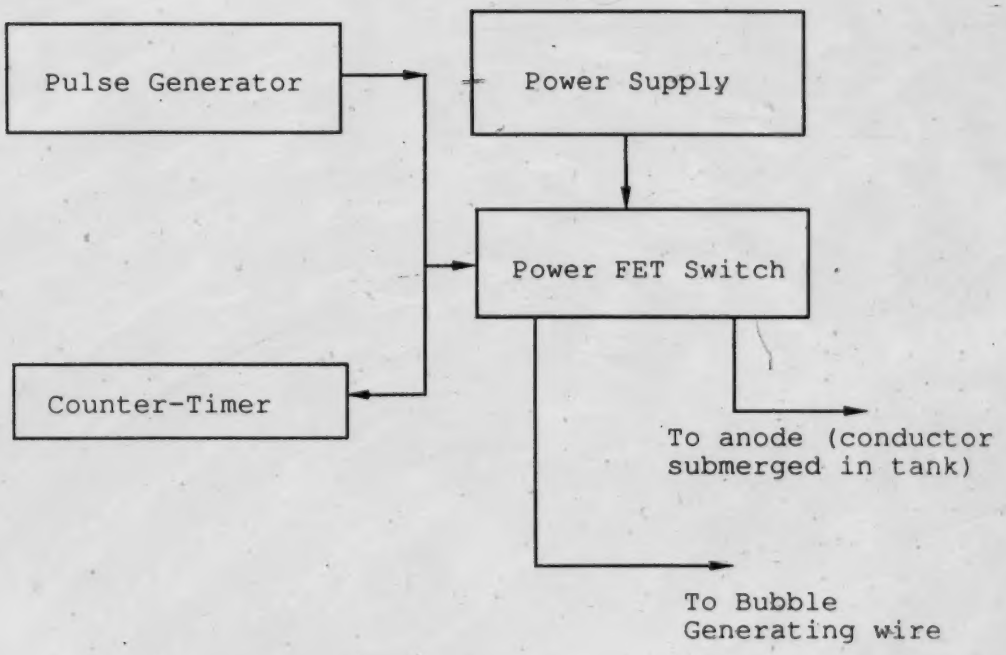

Figure 3.3 Schematics of the Hydrogen Bubble Apparatus

Plate 3.4 The Hydrogen Bubble Apparatus

3.3.3.2 Pulsing Unit

This solid state unit varies the pulse duration and the frequency. The pulse duration option varies the amount of time during which the current is actually passed. This can be adjusted by observing the hydrogen bubble lines as they generate. The coarse frequency adjustment is positioned at 4 to 50 Hz. The fine adjustment can then be made to position at the desired frequency often determined by trial. While making any of these adjustments, it has to be made sure that the voltage unit is set to zero. Otherwise a sudden surge of current could burn the fuse in the pulsing unit.

3.3.4 Advantages and Limitations

The hydrogen bubble technique is normally suitable for velocity in the range of 0.1 to 15 cm/s. Since the range of velocity in this study was low (0.7 to 6.48 cm/s), this technique gave fairly good results. However, there are many advantages as well as disadvantages to using this method.

3.3.4.1 Advantages

1. Hydrogen bubbles do not contaminate the water as much as dye or other tracers.
2. Hydrogen bubbles, unlike dyes, do not lose their identities in wakes or turbulent flows.
3. The wires, being very fine, do not provide significant wake effects.

4. It provides simultaneously the velocity field and a visual image of the flow (plate 3.5).

(Pande, 1975)

3.3.4.2 Limitations

Measurement made using this technique has uncertainties as well (Pande, 1975).

1. Measurements of Δx on photograph (accuracy in this experiment was 0.1 mm)
2. Measurements could only be made of centreline velocities and none for the region of flow occupied by the shear layer.
3. Velocity at the nozzle exit was not measured due to the possibility of creating a short circuit.

3.4 EXPERIMENTAL PROCEDURE

3.4.1 Flow Visualisation

The first part of the study involved flow visualisation. It was intended to find out visually with the help of dye how the flow behaved in the vicinity of the nozzle. Initially, an approximate length of the flow development region was determined by injecting dye from two edges of the nozzle and observing photographically how the shear layer penetrated the central region. Plate 3.3 shows an example. These observations were compared with similar observations of a pure jet. The behaviour of the vortices

Plate 3.5 Typical Hydrogen Bubble Lines F_o= 0.86

shed from the nozzle were also studied by colouring the buoyant jet (Plate 3.6).

3.4.1.1 Inflow Study

One of the primary concerns in dealing with a low Froude number buoyant jet is that of inflow. The presence of a critical Froude number proposed by several authors had to be investigated with the available set-up. This possibility was observed by running the dye-coloured buoyant jet and increasing the discharge until the inflow stopped.

3.4.2 Buoyant Jet Experiments

These runs were conducted especially for the measurement of the centreline velocity. Measurements were made at positions along the axis at multiples of the diameter. Positions ranged from 0.5D to 6D. For measurement using hydrogen bubbles, two to three photographs were taken at each section and the velocity averaged. The frame with the tungsten wire was attached to the bottom of a point gauge which was mounted on a traverse. The point gauge provided the vertical movement and, if needed, the traverse provided the lateral movement.

The experiments were carried out using the city water supply. The tank was filled and allowed to stand for more than an hour in order to damp the eddies and circulation in the tank.

Plate 3.6 Flow Visualisation of a Buoyant Jet Showing Ring Vortex Structure

The presence of buoyancy in the experiment required an accurate measurement of the temperature as well as maintenance of a steady condition in the plume. After issuing from the nozzle, the discharge rose to the surface and overflowed into the overflow channel (Fig 3.1d). This, however, didn't prevent the slow contamination of the ambient water. Thus measurements had to be made before the contamination diffused downwards close to the region defined by the potential core. Table 3.1 gives a list of the relevant parameters involved in the runs. Here T_a is the ambient temperature and T_p is the temperature of the buoyant jet in °C

In order to prepare a steady condition, warm water was circulated in the line *efhk* (Fig. 3.1) before the gate at the nozzle was opened. On opening the gate, measurements were made only after allowing about a minute for the jet to stabilise.

Table 3.2 The Relevant Parameters for the Experiment

Run No.	Ta (C)	Tp (C)	Nozzle Dia. D (cm)	Discharge (Lpm)
1 - 5	Test	runs	-	-
6	16.27	29.86	10	27.48
7	20.29	31.11	5	2.40
8	19.58	32.57	5	4.80
9	18.91	32.19	5	7.20
10	17.99	30.45	5	6.60
11	17.14	30.74	5	1.23
12	17.08	37.20	5	5.28
13	10.90	25.83	2.5	0.20
14	10.90	25.83	2.5	0.40
16	9.66	22.70	2.5	0.37
17	7.55	17.79	5	0.50
18	7.55	18.40	5	1.02
19	6.67	16.50	5	1.26
20	6.80	14.00	5	3.02
21	7.00	18.20	5	3.78
23	7.70	18.20	10	10.02
24	7.70	18.20	10	12.00
25	7.70	18.20	10	13.80
26	6.70	18.30	10	8.50
27	6.70	18.30	10	11.00
28	6.70	18.30	10	15.00
29	7.20	17.50	2.5	1.00
30	6.90	17.90	2.5	0.12
31	6.90	17.90	2.5	0.20
32	6.90	17.9	2.5	0.30

(Lpm = Litres per minute)

4. ANALYSIS OF EXPERIMENTAL RESULTS

4.1 General Equations

Consider a circular buoyant jet of diameter d issuing vertically upwards from a nozzle with an almost uniform velocity of U_o. Let ρ_o be the mass density of the jet at the nozzle and let ρ_a be the mass density of the uniform ambient of large extent surrounding the jet. If it is assumed that ρ_a is only slightly larger than ρ_o, we can make the Boussinesq approximation:

$$\frac{\rho_o}{\rho_a} = 1 - \frac{\Delta\rho_o}{\rho_a} \simeq 1 \qquad [4.37]$$

It is assumed that mixing around the emerging jet is essentially turbulent except perhaps in the immediate vicinity of the nozzle. The turbulent mixing around the jet leads to the formation of an axisymmetric turbulent buoyant shear layer surrounding an essentially non-turbulent potential core.

In the potential core, the axial velocity u_m increases with the axial distance due to the built-in buoyancy. However, its radial extent is continuously decreasing due to the penetration of the turbulent mixing as well as due to the thinning of the jet due to buoyancy-induced acceleration. Let L be the axial distance at which the potential core disappears and let this be referred to as the

length of the potential core. The flow region from the nozzle to the end of the potential core is generally referred to as the region of developing flow.

For the turbulent buoyant jet the continuity equation is approximately written as

$$\frac{\partial ru}{\partial x} + \frac{\partial rv}{\partial r} = 0 \qquad [1.2]$$

where u and v are the time averaged velocities at any point (x,r) in the axial (x) and radial direction respectively. The Reynolds equations can be reduced to

$$u \frac{\partial u}{\partial x} + v \frac{\partial u}{\partial r} = \frac{1}{\rho_a} \frac{1}{r} \frac{\partial r\tau}{\partial r} + \frac{g\Delta\rho}{\rho_a} \qquad [1.9]$$

where τ is the turbulent shear stress, g is the accleration due to gravity , $\Delta\rho$ is equal to $(\rho_a - \rho)$, ρ being the time-averaged density at any point. In writing Eq. 1.9, the use of slender flow as well as Boussinesq approximation has been made and if necessary, ρ_a could be replaced by ρ_o the density of the jet fluid at the nozzle.

If $\hat{c} = g\Delta\rho$, the conservation equation for $\hat{c}$ can be written as

$$u \frac{\partial \hat{c}}{\partial x} + v \frac{\partial \hat{c}}{\partial r} = \frac{1}{r} \frac{\partial}{\partial r} \left(r\epsilon \frac{\partial \hat{c}}{\partial r} \right) \qquad [1.10]$$

where ϵ is the eddy diffusivity in the radial direction which has been assumed constant over the section.

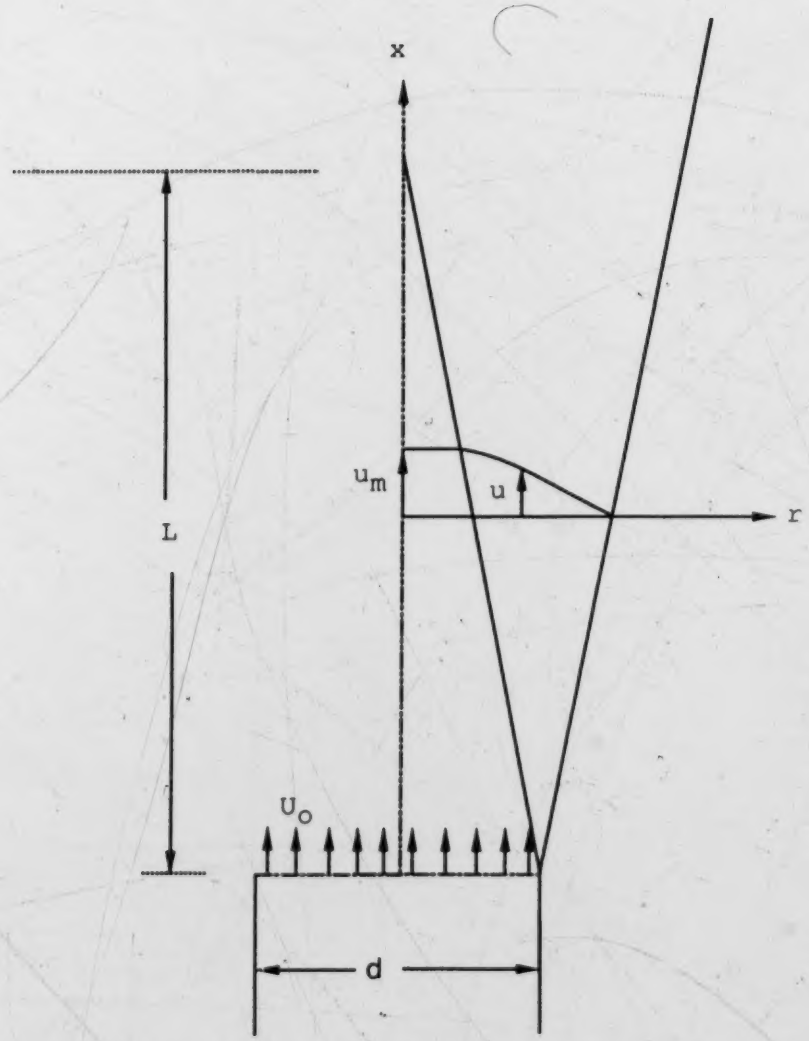

Figure 4.1 Definition Sketch of the Potential Core

4.1.1 Potential Core

One of the main assumptions in the potential core is that the turbulence is assumed to be negligible therefore the term with τ vanishes. The momentum equation 1.9 would therefore reduce to:

$$u \frac{\partial u}{\partial x} + v \frac{\partial u}{\partial r} = \frac{g \Delta\rho}{\rho_a} \qquad [4.38]$$

On the axis of the buoyant jet, since v = 0 Eq. 4.38 further reduces to:

$$u \frac{\partial u}{\partial x} = \frac{g \Delta\rho}{\rho_a} \qquad [4.39]$$

If u_m is the value of u on the axis of the jet at any distance x from the nozzle, Eq. 4.39 can be written as:

$$\frac{d}{dx}\left(\frac{u_m^2}{2}\right) = \frac{g \Delta\rho_o}{\rho_a} \qquad [4.40]$$

where $\Delta\rho_o = \rho_a - \rho_o$

On Integrating Eq. 4.40:

$$u_m^2 = U_o^2 + 2g \frac{\Delta\rho_o}{\rho_a} x \qquad [4.41]$$

where U_o is the velocity at the nozzle.

Eq. 4.41 can be written as:

$$\left[\frac{U_m}{U_o}\right]^2 = 1 + \frac{2}{F_o^2}\,\frac{x}{d} \qquad [4.42]$$

where:

$$F_o = \frac{U_o}{\sqrt{g\ (\Delta\rho_o/\rho_a)\ d}}$$

where d is the diameter of the jet as it leaves the nozzle.

At the end of the potential core of length L if the value of u_m is U_m, the Eq. 4.42 gives

$$\left[\frac{U_m}{U_o}\right]^2 = 1 + \frac{2}{F_o^2}\,\frac{L}{d} \qquad [4.43]$$

The length of the potential core would depend upon the narrowing of the jet due to the built-in acceleration caused by buoyancy as well as the internal penetration of the surrounding axisymmetric shear layer. If the Reynolds number of the buoyant jet at the nozzle is large enough for the viscous effects to be negligible, then, based on our understanding of the turbulent shear layers, it would appear that L/d will be a function of only F_o and as a result (U_m/U_o) will be a function of only F_o. Further, since for large values of F_o the effects of buoyancy will be negligible, one would expect U_m/U_o to decrease continuously with F_o.

If Eq. 4.43 is equated with Eq. 1.24 for the end of the potential core, the following implicit equation can be

written for the diameter based densimetric Froude number.

$$\left[1 + \frac{2}{F_o^2}\frac{L}{d}\right]^{1/2} = \left[\frac{64.75}{F_o^2\,(L/d)} + \frac{223.25}{(L/d)^3}\right]^{1/3} \qquad [4.44]$$

4.2 Inflow Mechanism

As mentioned earlier, the problem of inflow was unavoidable because of the low range of Froude number of the study. For all the runs, where the densimetric Froude number was less than unity, inflow was present. It was observed that the inflow was not concentrated to any one region of the nozzle but occurred randomly. The extent of inflow was also random. The observations of inflow were more qualitative than quantitative. It was not possible to record the depth of penetration because the experimental set up had no provisons for this.

A few runs were carried out with Cochineal dye coloured jets. The discharge was increased from a certain small amount where the inflow occurred to a point where the jet was visually observed to flow full. Table 4.1 gives the result of these observations.

One of the shortcomings of these observations was that there was enough room for the error of parallax because the nozzle was at least 0.6 m away from the jet tank wall. Furthermore, because of the mushroom shaped *puffing* nature of the buoyant jet at the nozzle at the low range of Froude number (Plate

3.6), the exact full-flow was reasonably difficult to determine. Table 4.1 Results of Inflow Study

D (cm)	T_a (°C)	T_p (°C)	Q (m^3/sec)	F'_o
5	6.0	22.3	0.000067	1.03
5	6.0	22.3	0.000067	1.03
10	8.4	18.9	0.00033	1.10
10	7.5	26.1	0.000045	1.03
10	7.5	21.5	0.00004	1.13

4.3 Effective Diameter

A direct consequence of the inflow was that the nozzle was not flowing full. As a result of this, an effective diameter d of the nozzle had to be evaluated. The available data at hand was the discharge through the nozzle measured with the rotameter and the centreline velocity of the buoyant jet at different locations along the jet axis.

The effective area of the buoyant jet at the nozzle was evaluated by dividing the discharge by the velocity at the nozzle. However, one of the limitations of the hydrogen bubble technique was that measurements could not be made at

the nozzle because of the danger of short circuiting the high voltage with the base of the tank which was made of aluminum sheet.

This problem was solved by graphically evaluating the velocity at the nozzle. The square of the measured velocity at different locations along the axis of the buoyant jet for each run were plotted against x/D in accordance with Eqn. 4.41. The y axis intercept gave the nozzle velocity squared. Appendix B gives the plots for all the runs from which the nozzle velocities were determined. The straight lines drawn through the data points have been done by visual inspection.

4.4 Velocity Field

Initially one of the aims of the study was to make turbulence measurements using the laser and also to make some velocity measurements in the shear layer. This possibility was overruled after encountering some optical problems with the laser. Some measurements of the centreline velocity have been made in the large Froude number range (Appendix C). Since the data rate was very low while using the laser, the measurement duration at times was more than 15 minutes. In some cases, when the discharge was large, the time was sufficient to pollute the surrounding ambient and thus fail to provide an ideal condition for the experiment.

The second alternative was to use the Hydrogen bubble method for the instantaneous velocity measurements. Plate 3.5 is a typical example of the Hydrogen bubble time lines.

As can be seen from the photograph, the boundary of the shear layer and the potential core was very hard to determine. Furthermore, because of density differences, the convection current caused the time lines to decay earlier in the boundary region and thus made the boundary visually indeterminate. Therefore only the velocity along the axis of the jet was measured. Table 4.2 gives the results of velocity measurement. Fig 4.1a through Fig 4.1y give the plot of the velocity against the axial distance from the nozzle. A smooth line has been drawn through the data points by visual inspection. Table 4.3 and 4.4 give the summary of the data and their analysis.

4.5 Potential Core

4.5.1 Length

One of the objectives of the study was to find the length of the potential core L from the observations on u_m. According to Eq. 4.41 u_m will increase from U_o at the nozzle upto the end of the potential core. But, perhaps for an additional distance of ΔL, u_m will, at least in principle, continue to increase till the decreasing buoyancy term is balanced by the increasing shear gradient term (Eq. 1.10). The length of the potential core has been determined by picking the maximum of the velocity from Fig. 4.2 . This result has been plotted in Fig. 4.3. At this time we are

Table 4.2 Measured Velocity (cm/s)

Run No.	X/D											
	0.4	0.5	1.0	1.5	2.0	2.5	3.0	3.5	4.0	4.5	5.0	6.0
6		8.24	10.27	10.46	11.69		12.80	10.46	9.54		11.75	9.11
7	5.18		7.26		7.60		7.56		7.38		6.63	
8	6.95		8.88		8.34		12.03		10.70		10.87	8.82
9	7.79		10.23		10.79		12.55		13.74		11.47	11.47
10			7.46		9.07				12.43		8.27	10.75
11	4.69		5.15		6.88		7.46		6.41		5.55	4.52
12	8.88		11.10		10.31		9.51		9.51		10.07	9.91
13			1.85		2.65		2.92		3.02		2.98	1.23
14			4.66		4.95		2.67		3.70		4.05	2.19
16			2.35		2.03	1.13	2.78	1.70	1.76	1.81	1.07	
17			2.14		2.90	2.20	2.20	2.29	1.35		2.69	2.04
18			3.39		4.32		3.14	4.27	2.57	2.87	2.69	
19			3.04		4.02		3.15	3.85	4.22		2.40	1.66
20			3.41		4.09		4.50		4.09		4.84	4.29
21			4.49		5.77		6.89		5.21		4.73	5.61
23			4.80		5.55		5.02		3.31		2.99	2.24
24			4.70		6.83		8.22		5.44		3.85	3.63
25			6.46		6.40		7.26		5.33		5.12	4.90
26		3.67	4.10		6.12		3.18		4.29		2.82	
27		4.29	5.69		5.39		3.68		5.75		3.43	
28		3.92	4.66		6.12		6.61		1.84		5.88	
29			4.35		4.35		5.58		6.20		6.15	5.82
30			1.51		1.80		0.71		1.47			
31			2.70		2.54		3.22		1.99		1.32	
32			2.18		2.84		1.89		1.80		1.70	

Table 4.3 Summary of Corrected Velocity, Diameter and Froude Number

Run No.	Vo (cm/s)	Comp. vel Uo (cm/s)	Nozzle Reynolds No.	Comp. Dia d (cm)	Corr. Fr. Fo	Um/Uo	L/d
6	5.84	6.48	7679	9.48	1.19	1.90	3.20
7	2.04	3.20	1641	4.00	0.95	2.40	2.80
8	4.07	5.30	3109	4.40	1.38	2.25	4.00
9	6.11	6.11	4191	5*	1.55	2.10	3.40
10	5.60	5.60	3300	5*	1.53	1.80	4.00
11	1.04	3.74	1250	2.64	1.30	1.90	5.00
12	4.50	6.92	4152	4.02	1.49	1.70	2.50
13	0.68	0.70	193	2.40	0.27	4.30	4.00
14	1.36	4.35	700	1.40	2.20	1.15	3.00
16	0.34	1.41	348	2.35	0.64	2.00	3.00
17	0.42	0.89	277.5	3.43	0.44	3.20	2.90
18	0.85	1.54	522	3.73	0.69	2.80	3.30
19	1.09	1.48	523	4.24	0.71	2.75	3.20
20	2.57	2.54	1016	5*	1.41	1.75	2.80
21	3.20	3.20	1491	5*	1.25	2.25	3.40
23	2.12	3.87	2603	7.40	1.25	1.45	3.00
24	2.55	2.55	2318	10.00	0.69	3.10	2.90
25	2.97	5.38	3605	7.37	1.74	1.35	3.25
26	1.80	3.24	2194	7.45	1.02	1.90	3.20
27	2.30	2.30	2091	10*	0.63	2.60	2.20
28	3.18	3.18	2891	10.00	0.86	2.10	3.00
29	3.40	3.40	739	2.50	1.97	1.80	4.50
30	0.40	1.58	181	1.26	1.25	1.10	4.00
31	0.68	2.02	264	1.44	1.50	1.50	4.80
32	1.02	1.18	248	2.31	0.69	2.37	2.50

* The computed diameter was larger than the nozzle dia. used

Table 4.4 Summary of Fo', Uo/Vo, and d/D

Run No.	Nozzle dia. D (cm)	Comp. dia d (cm)	Discharge (Lpm)	Vo cm/s	Comp. vel. Uo (cm/s)	Full Flow Fr No. (Fo')	Corr. Fr. No. Fo	Uo/Vo	d/D
6	10	9.48	27.48	5.84	6.48	1.05	1.19	1.11	0.95
7	5	4.00	2.40	2.04	3.20	0.65	0.95	1.57	0.80
8	5	4.40	4.80	4.07	5.30	1.09	1.38	1.30	0.88
9	5	5*	7.20	6.11	6.11	1.55	1.55	1.00	1.00
10	5	5*	6.60	5.60	5.60	1.53	1.53	1.00	1.00
11	5	2.64	1.23	1.04	3.74	0.26	1.54	3.60	0.53
12	5	4.02	5.28	4.50	6.92	0.87	1.49	1.54	0.80
13	2.5	2.40	0.20	0.68	0.70	0.26	0.27	1.03	0.96
14	2.5	1.40	0.40	1.36	4.35	0.52	2.20	3.20	0.56
16	2.5	2.35	0.37	0.34	1.41	0.15	0..64	4.15	0.94
17	5	3.43	0.50	0.42	0.89	0.17	0.44	2.12	0.69
18	5	3.73	1.02	0.85	1.54	0.32	0.69	1.81	0.75
19	5	4.24	1.26	1.09	1.48	0.48	0.71	1.36	0.85
20	5	5*	3.02	2.57	2.54	1.42	1.41	0.99	1.00
21	5	5*	3.78	3.20	3.28	1.25	1.25	1.03	1.00
23	10	7.40	10.02	2.12	3.87	0.59	1.25	1.83	0.74
24	10	10*	12.00	2.55	2.55	0.69	0.69	1.00	1.00
25	10	7.37	13.80	2.97	5.38	0.80	1.74	1.81	0.74
26	10	7.45	8.50	1.80	3.24	0.49	1.02	1.80	0.75
27	10	10*	11.00	2.30	2.30	0.63	0.63	1.00	1.00
28	10	10*	15.00	3.18	3.18	0.86	0.86	1.00	1.00
29	2.5	2.5*	1.00	3.40	3.40	1.97	1.97	1.00	1.00
30	2.5	1.26	0.12	0.40	1.58	0.23	1.25	3.95	0.50
31	2.5	1.44	0.20	0.68	2.02	0.38	1.50	2.97	0.58
32	2.5	2.31	0.30	1.02	1.18	0.56	0.69	1.16	0.92

* The computed diameter was larger than the nozzle dia used

Lpm = Litres per minute

Figure 4.2 (a-y) Variation of u_m/U_o With x/d for Buoyant Jets

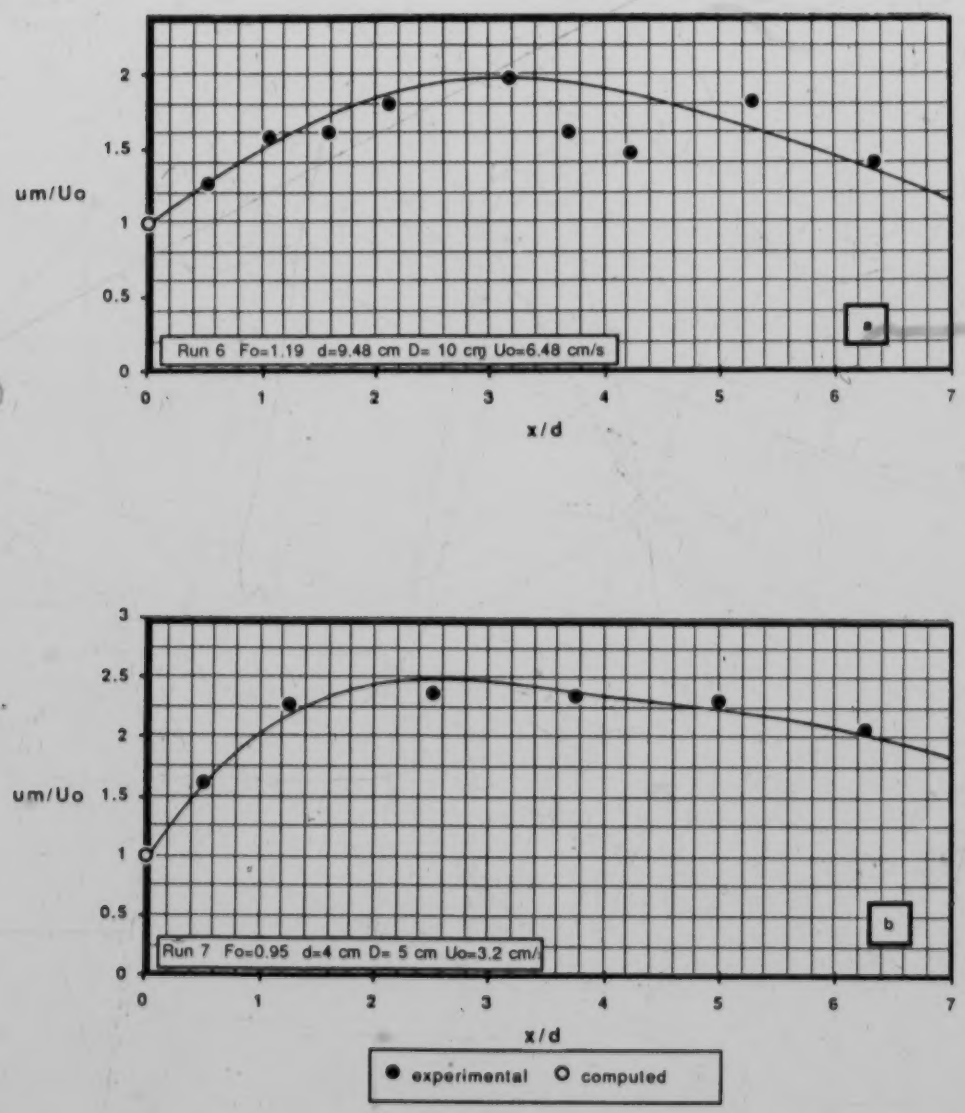

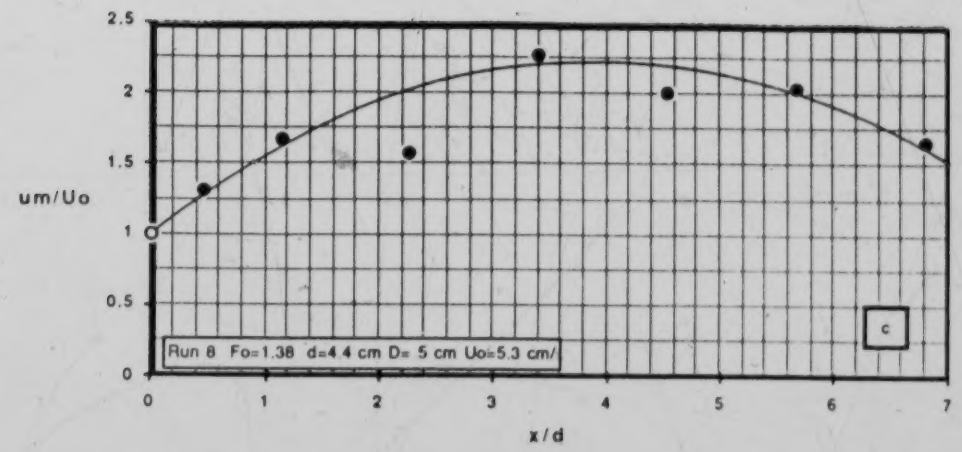
um/Uo
x/d
Run 8 Fo=1.38 d=4.4 cm D= 5 cm Uo=5.3 cm/
c

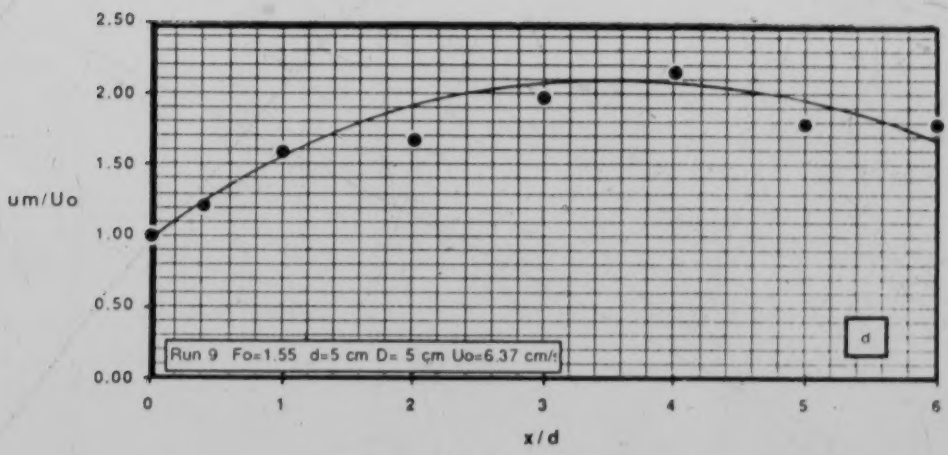
um/Uo
x/d
Run 9 Fo=1.55 d=5 cm D= 5 cm Uo=6.37 cm/
d

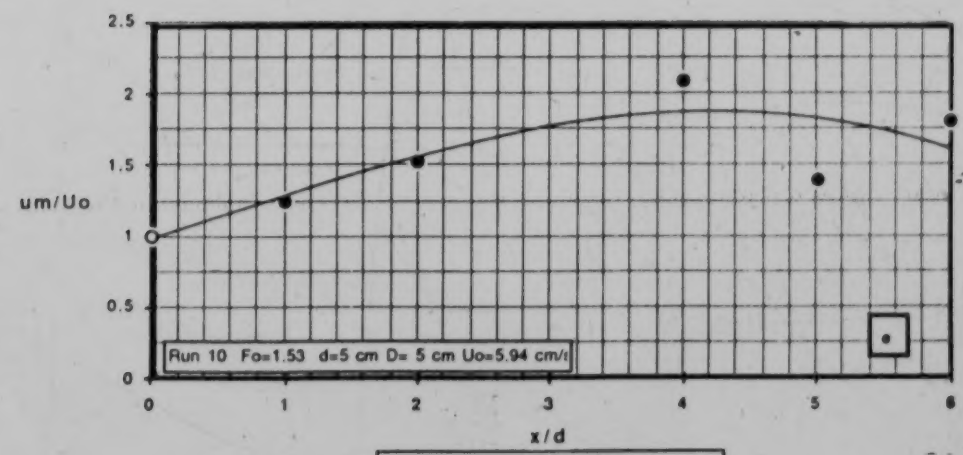
um/Uo
x/d
Run 10 Fo=1.53 d=5 cm D= 5 cm Uo=5.94 cm/
e
experimental
computed

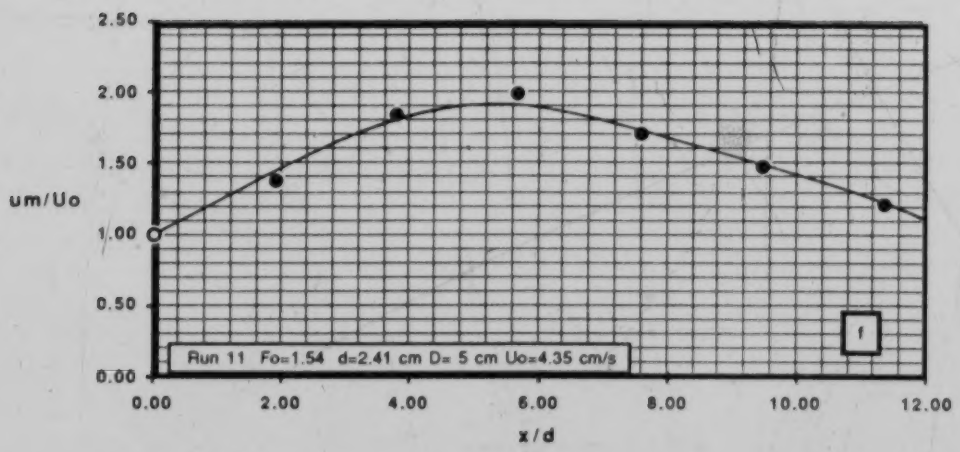
um/Uo
x/d
Run 11 Fo=1.54 d=2.41 cm D= 5 cm Uo=4.35 cm/s
f

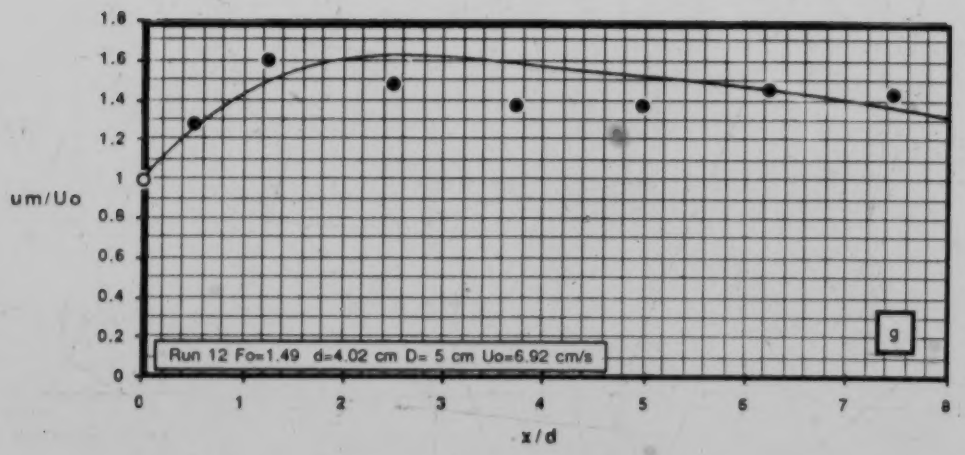
um/Uo
x/d
Run 12 Fo=1.49 d=4.02 cm D= 5 cm Uo=6.92 cm/s
g

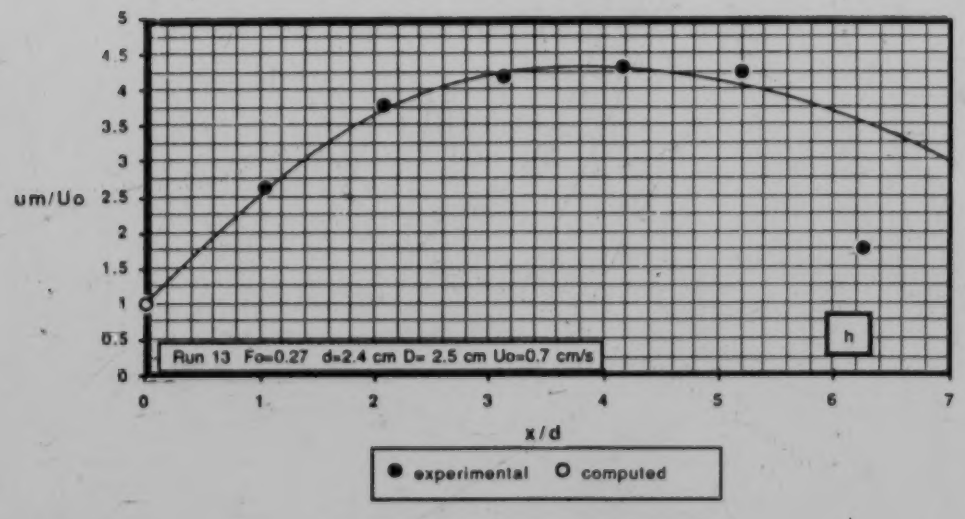
um/Uo
x/d
Run 13 Fo=0.27 d=2.4 cm D= 2.5 cm Uo=0.7 cm/s
h
experimental
computed

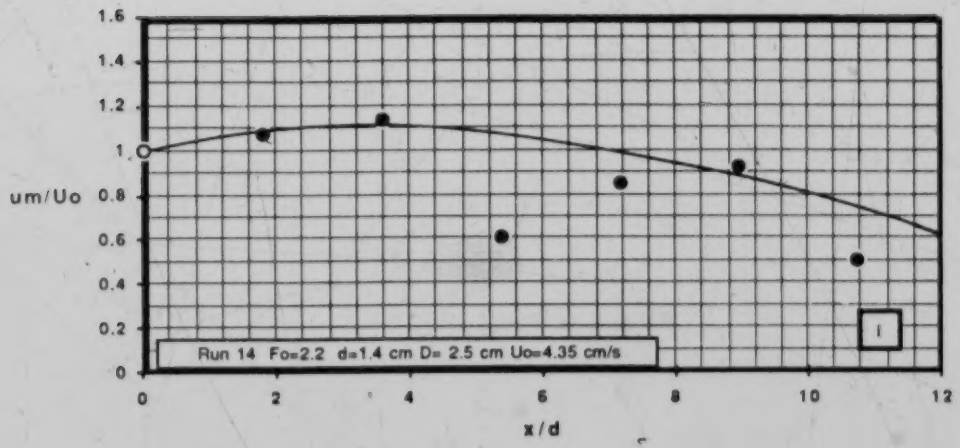
um/Uo
x/d
Run 14 Fo=2.2 d=1.4 cm D= 2.5 cm Uo=4.35 cm/s
i

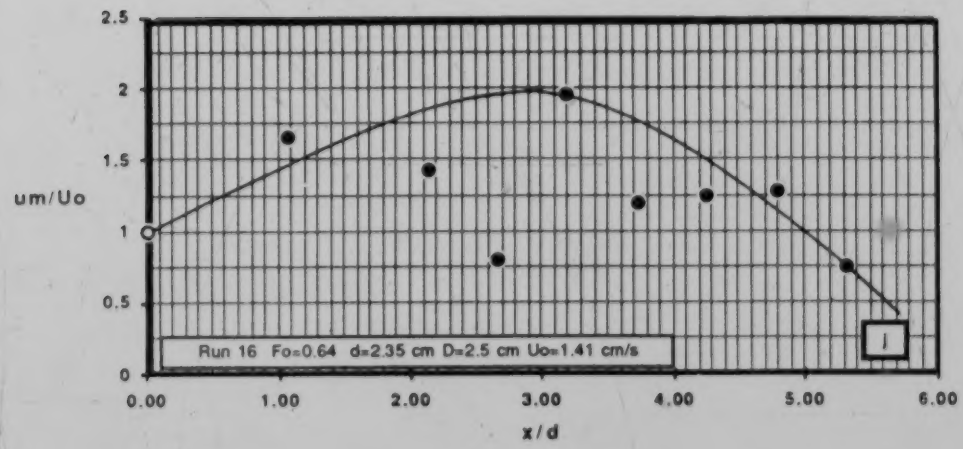
um/Uo
x/d
Run 16 Fo=0.64 d=2.35 cm D=2.5 cm Uo=1.41 cm/s
j

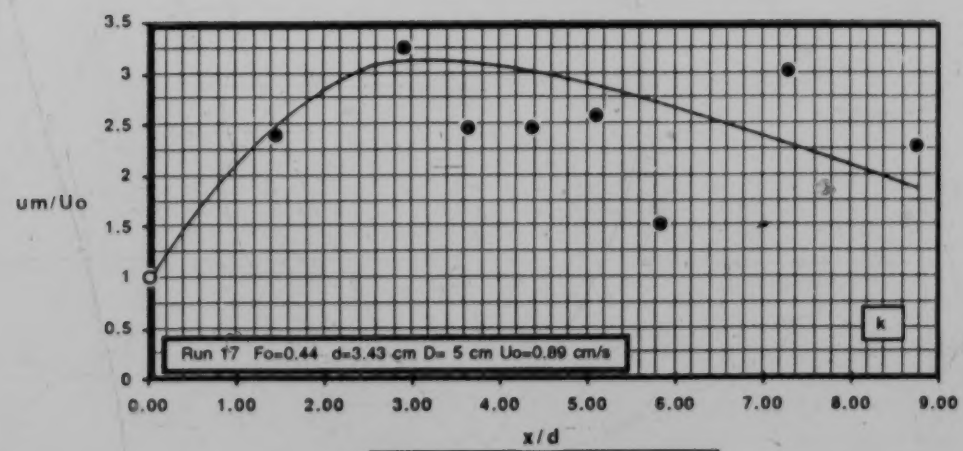
um/Uo
x/d
Run 17 Fo=0.44 d=3.43 cm D= 5 cm Uo=0.89 cm/s
k
experimental
computed

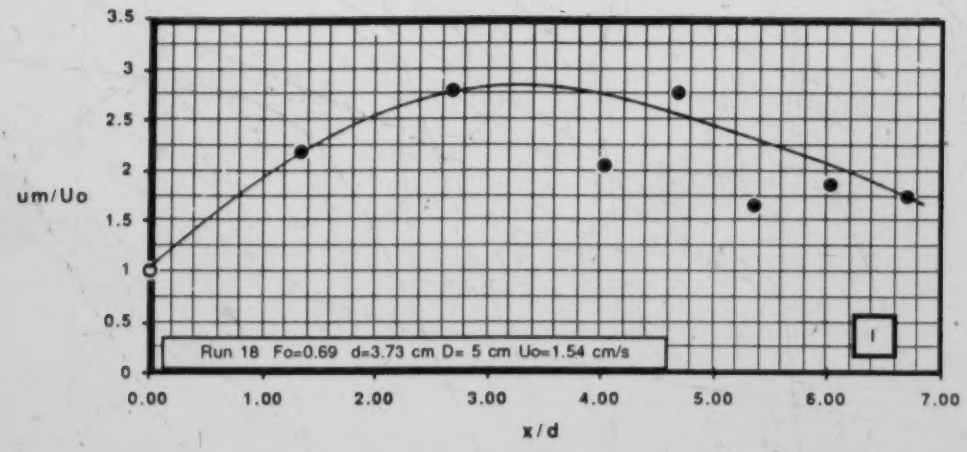
um/Uo
x/d
Run 18 Fo=0.69 d=3.73 cm D= 5 cm Uo=1.54 cm/s
l

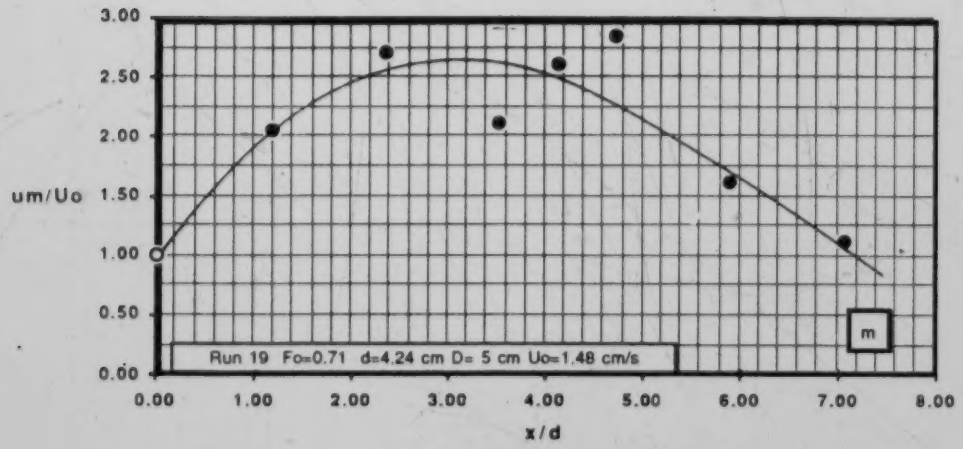
um/Uo
x/d
Run 19 Fo=0.71 d=4.24 cm D= 5 cm Uo=1.48 cm/s
m

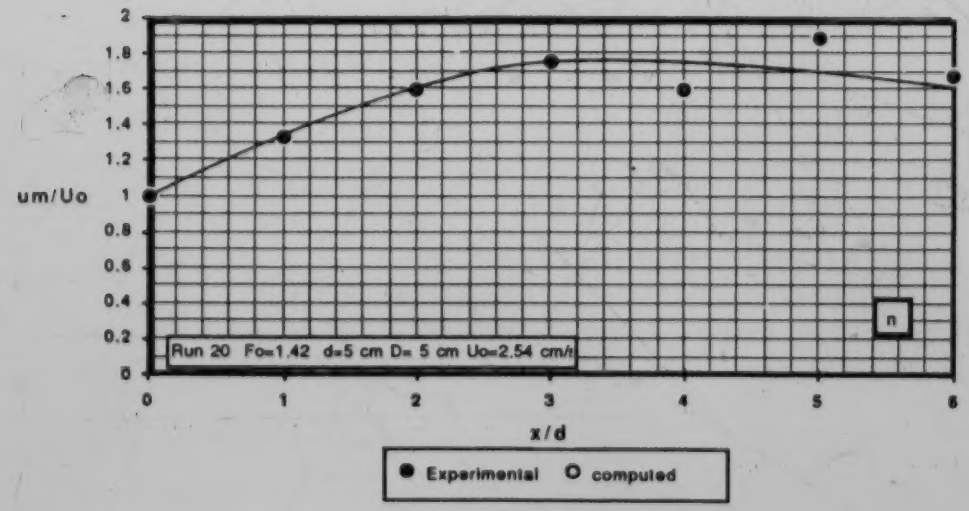
um/Uo
x/d
Run 20 Fo=1.42 d=5 cm D= 5 cm Uo=2.54 cm/s
n
Experimental
computed

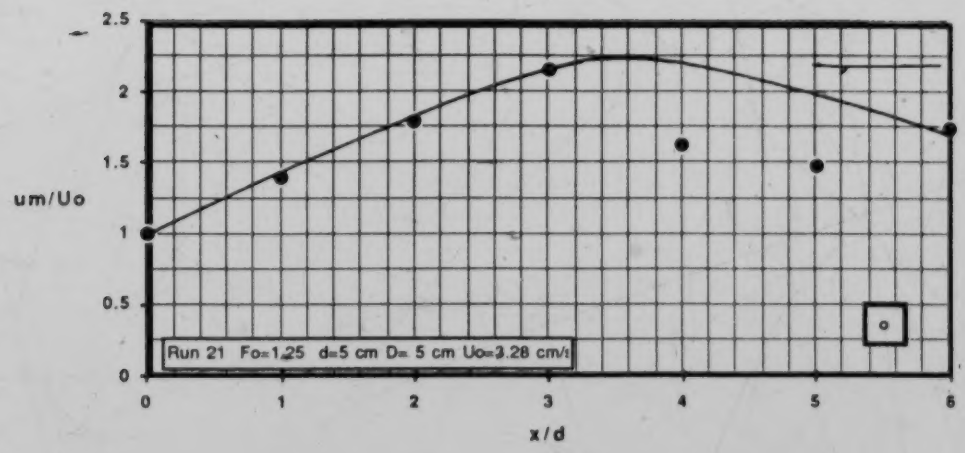
um/Uo
x/d
Run 21 Fo=1.25 d=5 cm D= 5 cm Uo=3.28 cm/s
o

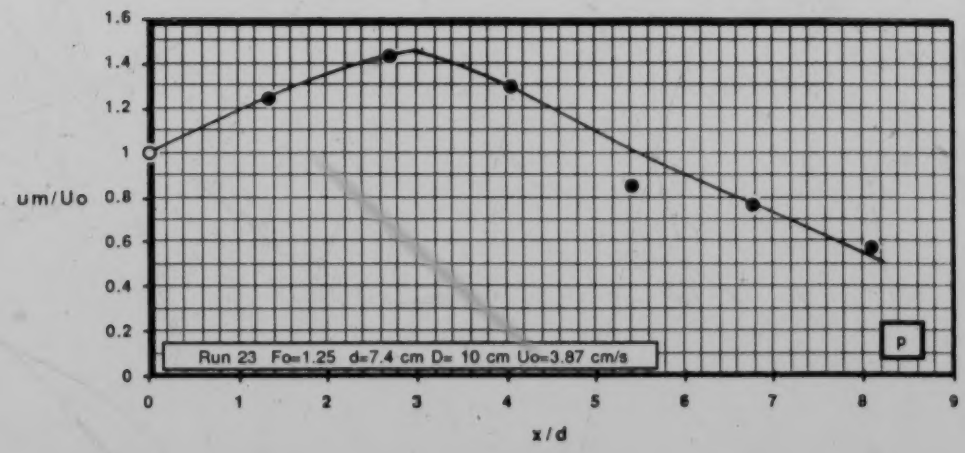
um/Uo
x/d
Run 23 Fo=1.25 d=7.4 cm D= 10 cm Uo=3.87 cm/s
p

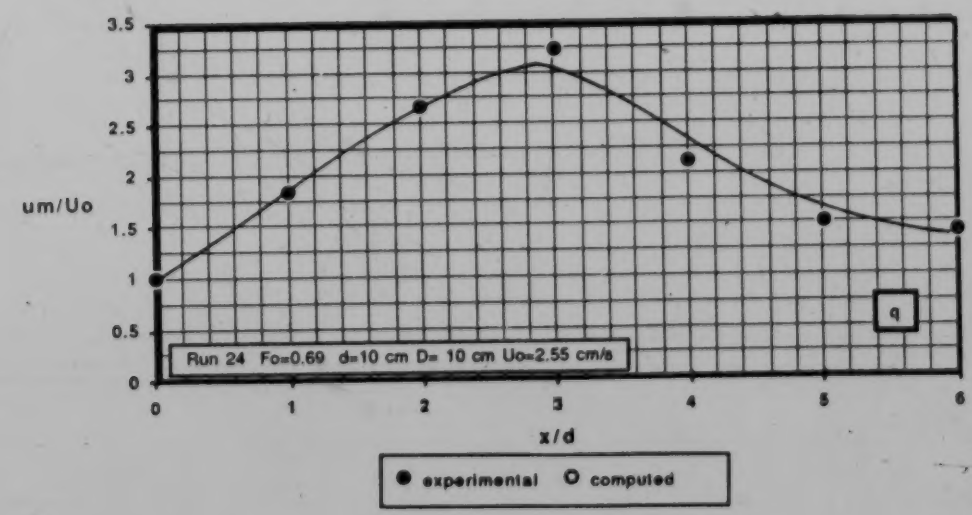
um/Uo
x/d
Run 24 Fo=0.69 d=10 cm D= 10 cm Uo=2.55 cm/s
q
experimental
computed

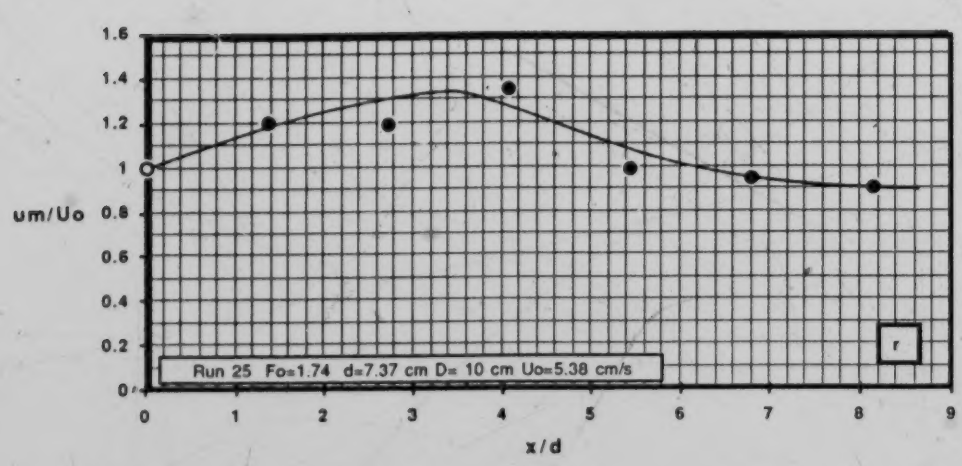
um/Uo
x/d
Run 25 Fo=1.74 d=7.37 cm D= 10 cm Uo=5.38 cm/s
r

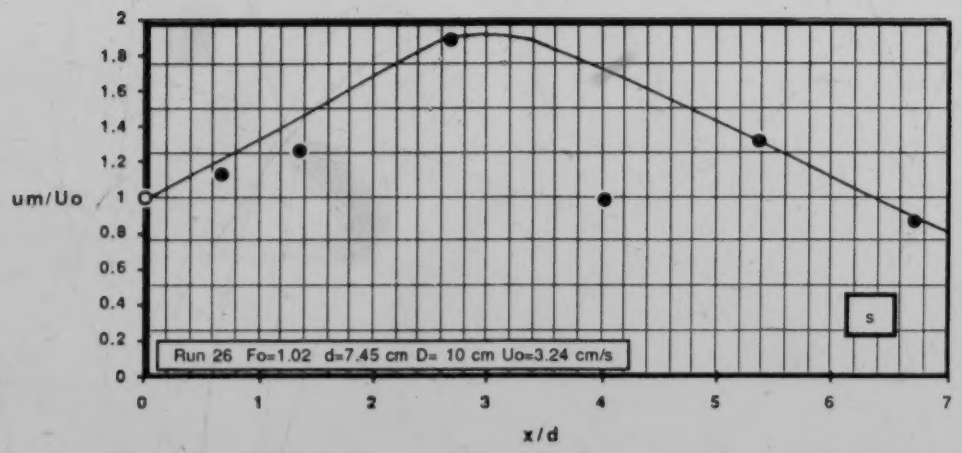
um/Uo
x/d
Run 26 Fo=1.02 d=7.45 cm D= 10 cm Uo=3.24 cm/s
s

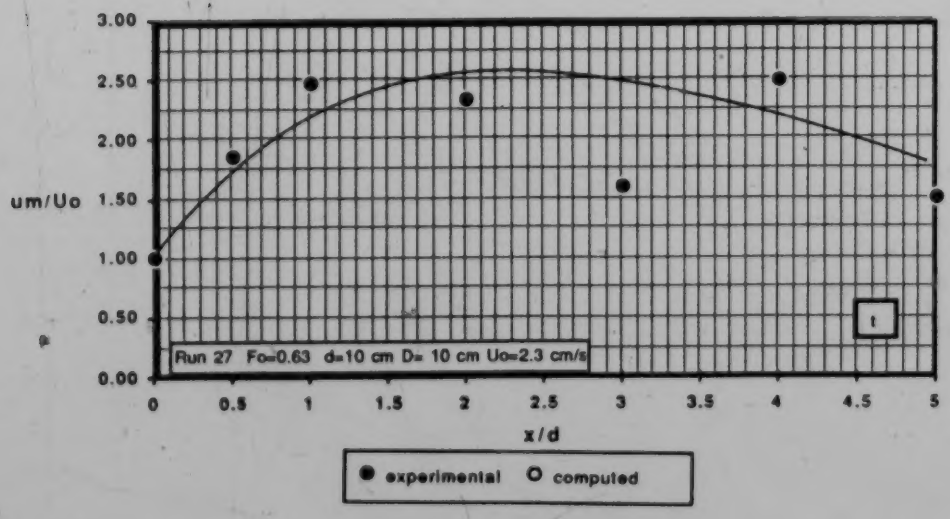
um/Uo
x/d
Run 27 Fo=0.63 d=10 cm D= 10 cm Uo=2.3 cm/s
t
experimental
computed

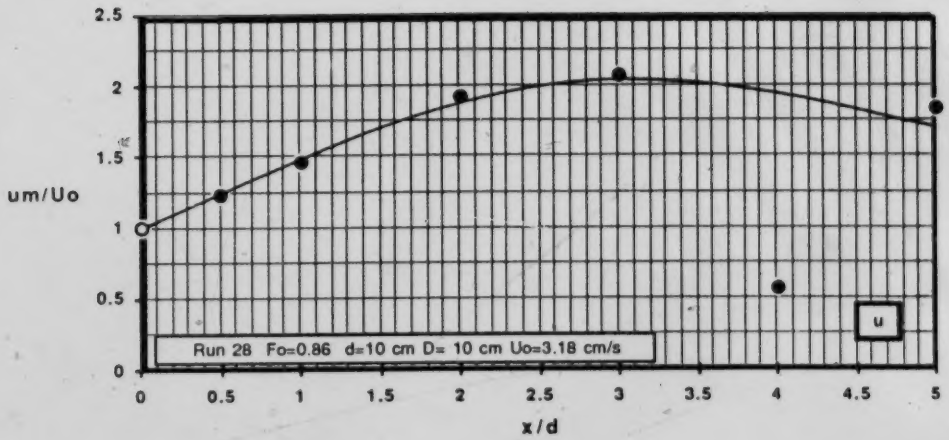
um/Uo
x/d
u
Run 28 Fo=0.86 d=10 cm D= 10 cm Uo=3.18 cm/s

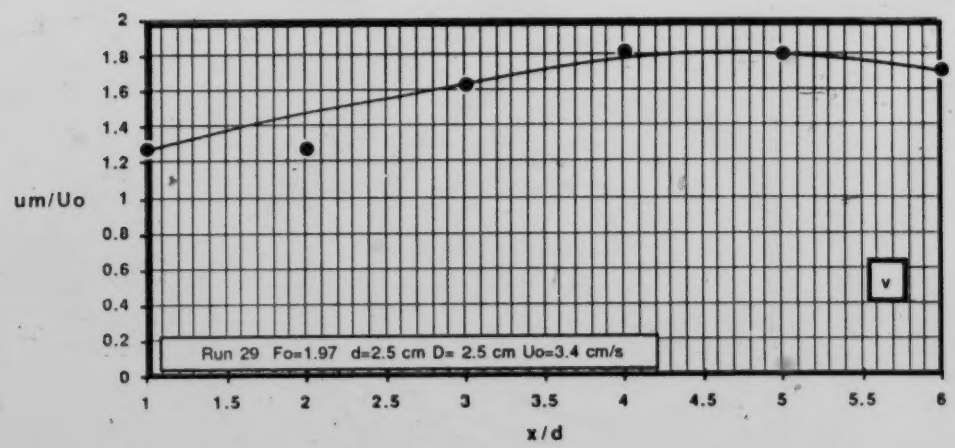
um/Uo
x/d
v
Run 29 Fo=1.97 d=2.5 cm D= 2.5 cm Uo=3.4 cm/s

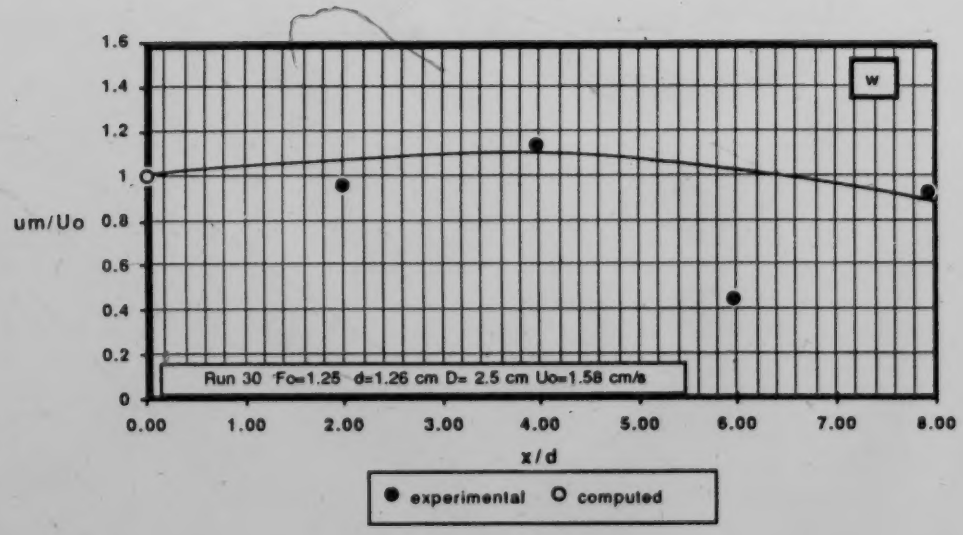
um/Uo
x/d
w
Run 30 Fo=1.25 d=1.26 cm D= 2.5 cm Uo=1.58 cm/s
experimental
computed

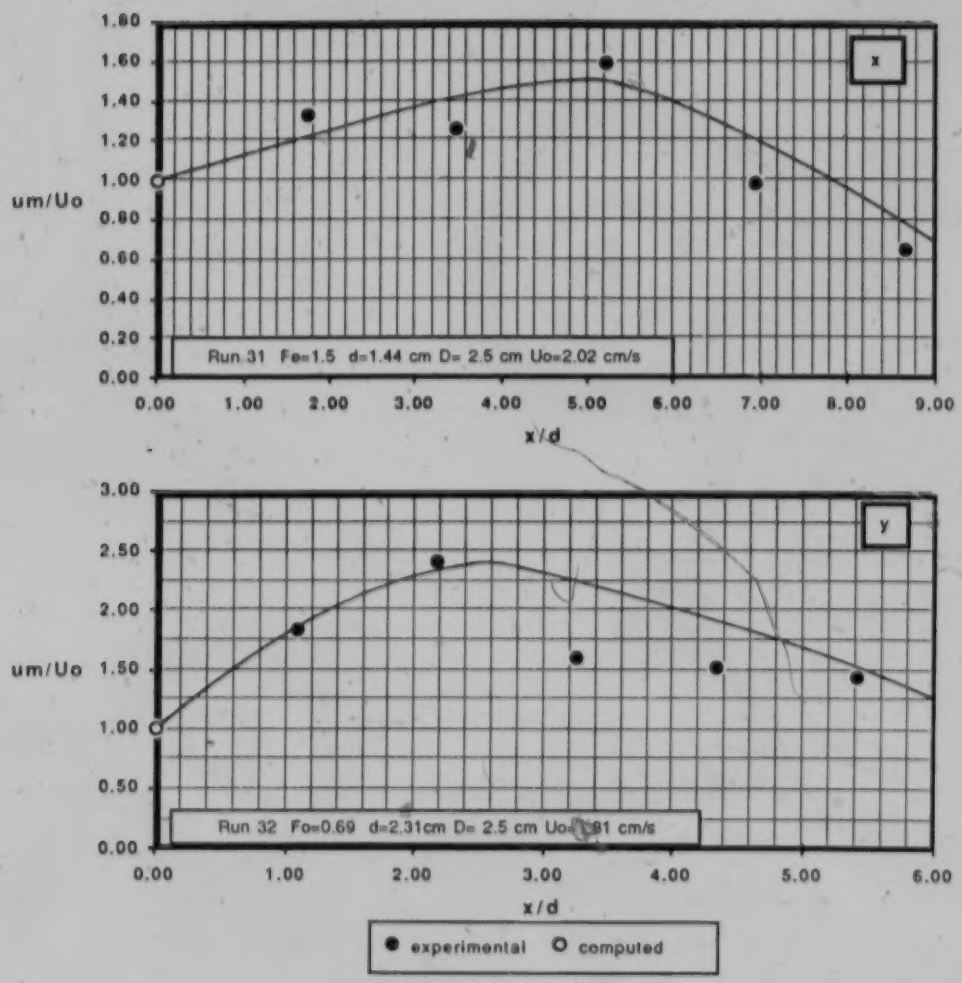
x
um/Uo
1.80
1.60
1.40
1.20
1.00
0.80
0.60
0.40
0.20
0.00
Run 31 Fo=1.5 d=1.44 cm D= 2.5 cm Uo=2.02 cm/s
0.00 1.00 2.00 3.00 4.00 5.00 6.00 7.00 8.00 9.00
x/d
y
um/Uo
3.00
2.50
2.00
1.50
1.00
0.50
0.00
Run 32 Fo=0.69 d=2.31cm D= 2.5 cm Uo=1.81 cm/s
0.00 1.00 2.00 3.00 4.00 5.00 6.00
x/d
experimental
computed

assuming that ΔL is very small compared to L and hence the location of U_m is taken as the end of the potential core. Therefore, the measured L will be somewhat larger than the actual length of the potential core. It is evident from Fig. 4.3 that the length of the potential core is dependent on the exit densimetric Froude number and is apparently contrary to the assumption that the length of the potential core in a buoyant jet is equal to that in a jet. Eq. 4.44 is also plotted in Fig. 4.3 and even though it predicts the trend correctly, the predicted values are somewhat higher than the experimental results.

4.5.2 Maximum Velocity

A very interesting result is that of the effect of buoyancy on the flow in the potential core. Fig. 4.4 shows that with increasing buoyancy i.e. decrease in F_o the velocity at the end of the potential core increases considerably from the velocity at the nozzle. Here again, Eq. 4.43 predicts the trend correctly but the velocity is slightly overpredicted. This is especially true in the lower Froude number range.

4.6 Results of Inflow

Table 4.3 shows that after the diameter has been corrected and a new full flow Froude number established based on the corrected velocity, F_o fails to show up as

Figure 4.3 Variation of L/d with Fo

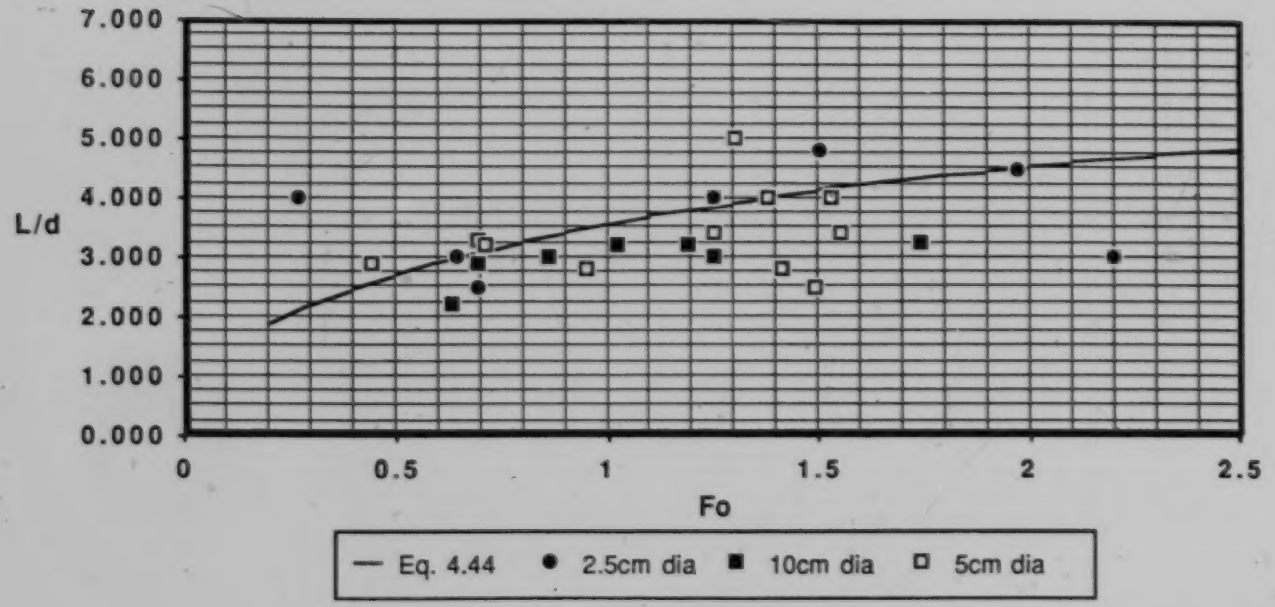

Figure 4.4 Axial Variation of Um/Uo with Fo

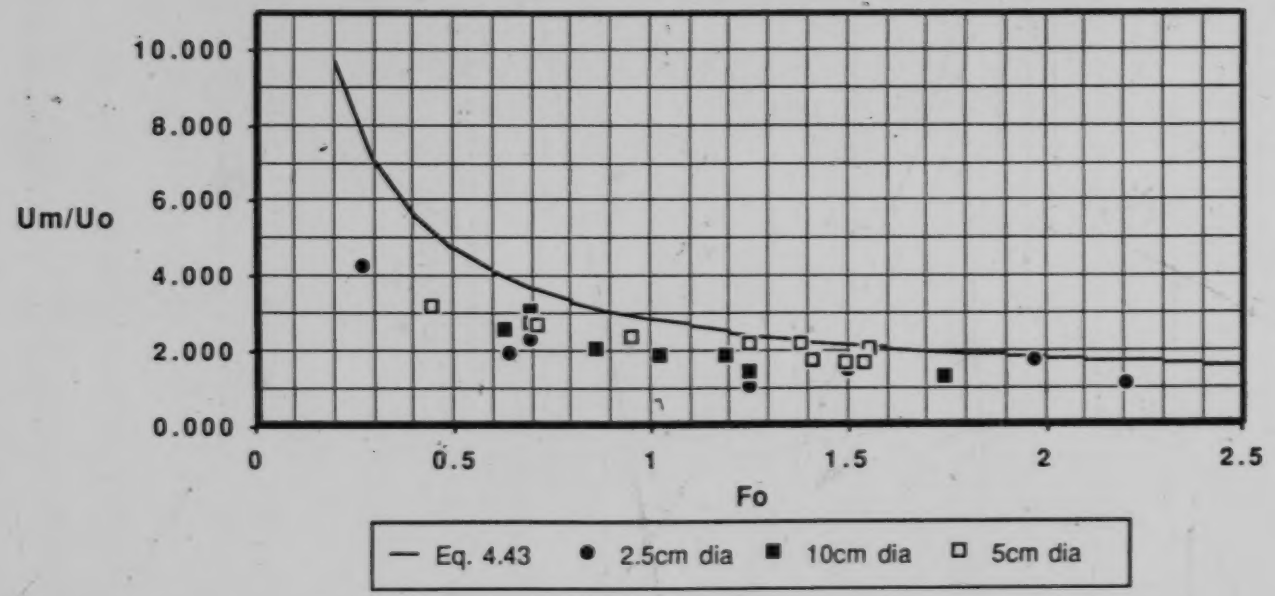

unity. This indicates the dependence of inflow on conditions other than Froude number alone.

Figure 4.5 shows the variation of d/D with the full flow exit Froude number. Knowing the discharge and the nozzle size, the area occupied by the jet can be predicted. A smooth curve drawn through the data points show that full flow starts at an approximate nozzle Froude number of 1.2.

Fig. 4.6 and Fig. 4.7 give further information on the prediction of the nozzle velocity and the jet Froude number with the information available on full flow condition. Fig. 4.6 is a plot of the variation of F_o with F_o'. A line has been drawn where $F_o = F_o'$. For the lower Froude number range, because of larger inflow and thus a reduction in the effective diameter, one would expect F_o to be larger than the full flow Froude number F_o'. This trend is clear from Fig. 4.6. All the data points lie above the $F_o = F_o'$ line. There is, however, a large scatter in the data points and any characteristic curve through them would be merely speculative. The data for F_o' greater than 1.2 seem to fall clearly on the bold line confirming the full flow condition for F_o greater than 1.2.

Fig. 4.7 shows the variation of U_o/V_o with F_o'. An approximate curve has been fitted through the data points. This allows for the prediction of the actual nozzle velocity of the buoyant plume for the known discharge. The data for the 2.5 cm nozzle shows some scatter. This could very well be because of the lower degree of accuracy involved with

Figure 4.5 Variation of d/D with Fo'

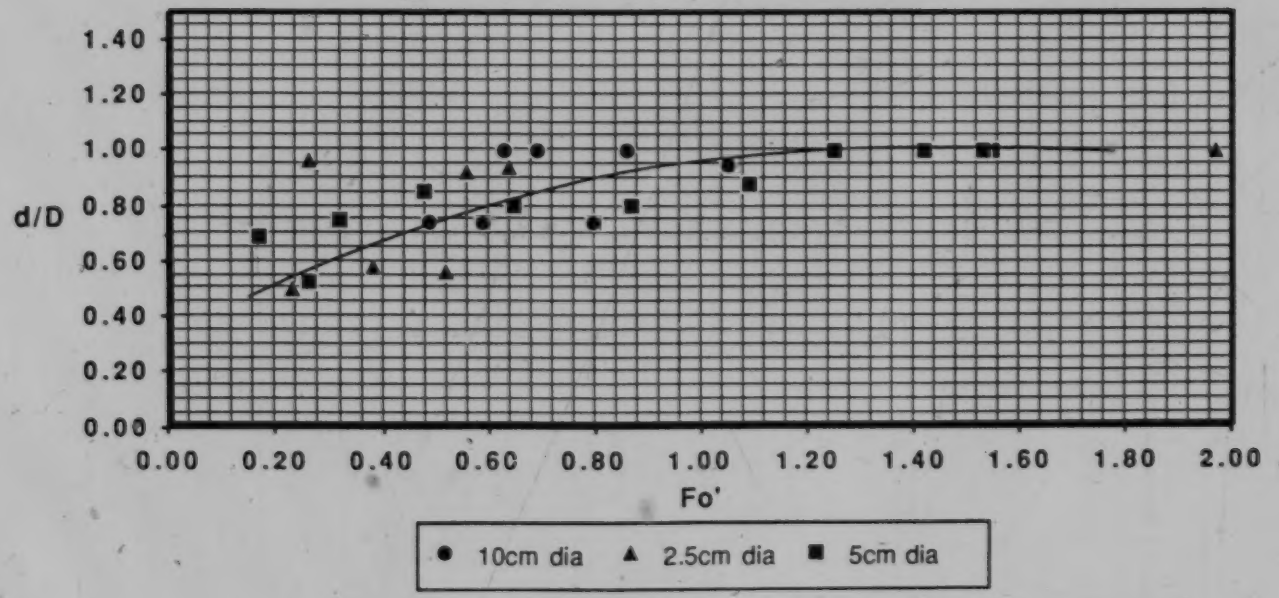

Hydrogen bubble measurements in this nozzle size due to the finer time lines. Fig. 4.7 also shows U_o/V_o approaching unity at F_o' of 1.2.

Figure 4.6 Variation of Fo with Fo'

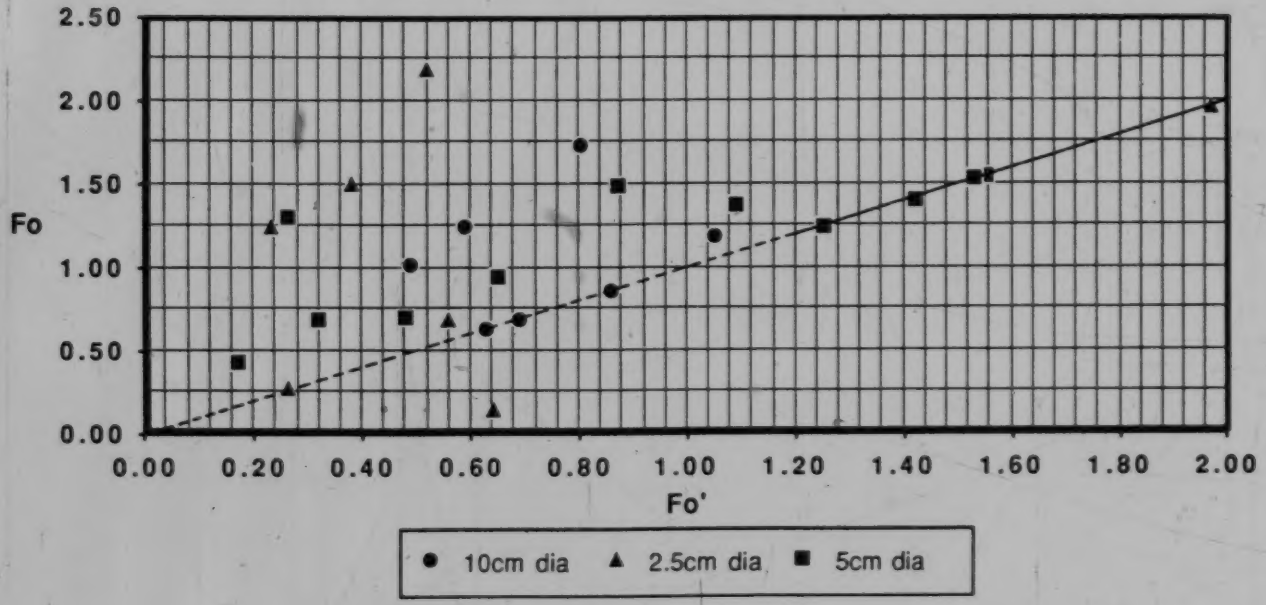

Figure 4.7 Variation of Uo/Vo with Fo'

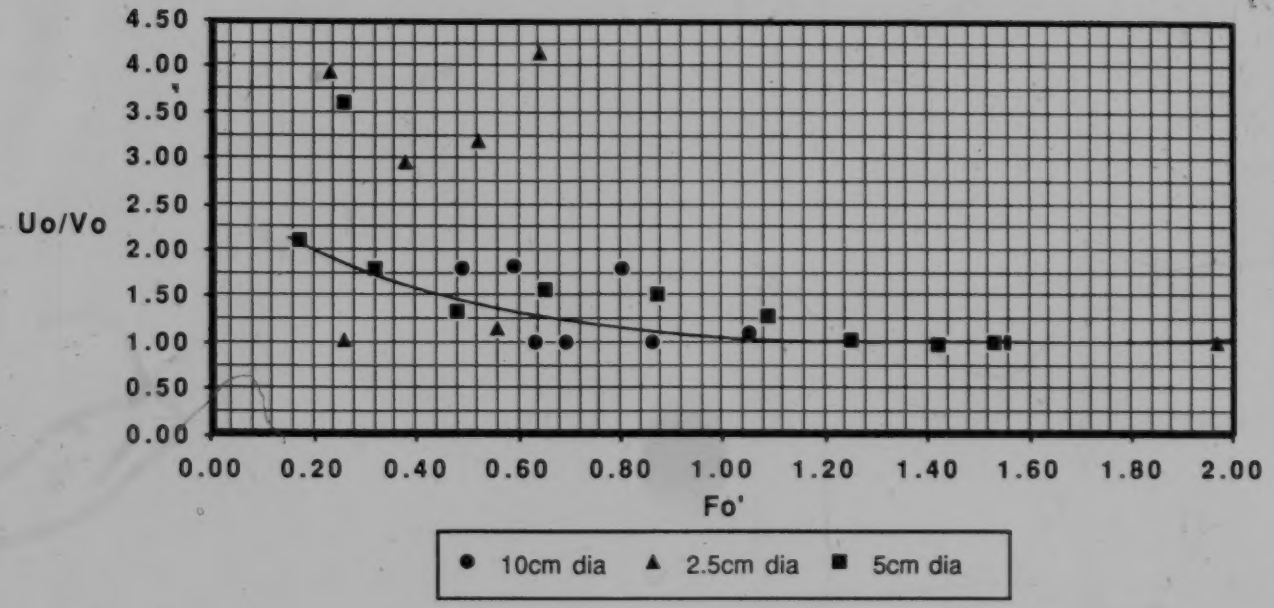

5. CONCLUSIONS AND RECOMMENDATION

5.1 Conclusions

An expression for the centreline velocity in the potential core has been developed by integrating the Reynolds Equation and assuming it to be free of turbulent shear.

A relation for the length of the potential core has been developed by equating the expression valid for the potential core with the expression for the fully developed region. This also allows for the prediction of the maximum velocity in the potential core at low Froude number.

The results of the measurements of the instantaneous velocities have been presented and the length of the potential core estimated from these measurements for densimetric Froude number in the range 0.27 to 2.2 .

A comparison of the results indicate that the analytical solution seems to slightly over-predict both the length of the potential core as well as the maximum velocity in the potential core. An important fact that has to be noted here is that the real end of the potential core is the point where the turbulence has finally penetrated to the centre of the jet (Fig. 4.8-a). As mentioned earlier, the position of the maximum velocity (Fig. 4.8-b) on the axis of the jet is only a practical estimate of the length of the potential core and it probably overestimates the length by about half a nozzle diameter. The length of the potential

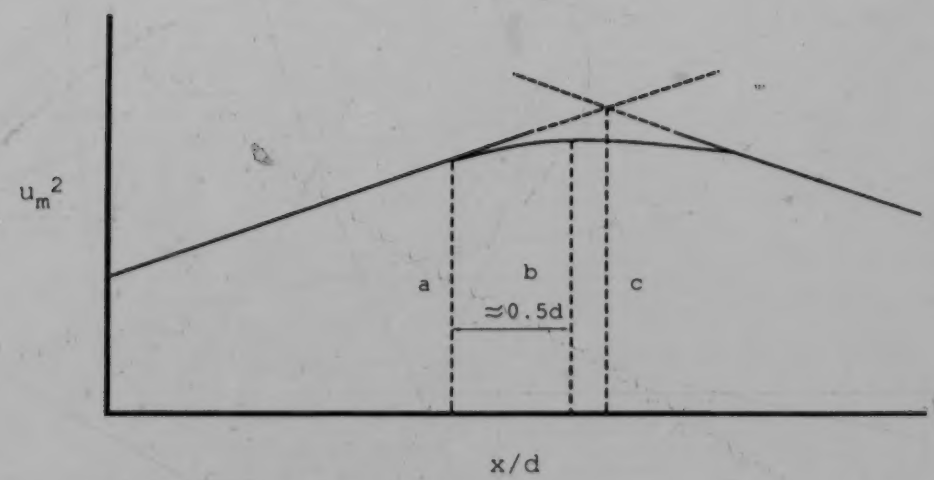

Figure 5.1 Potential Core Determination of a Buoyant Jet

core estimated according to equation 4.44 (Fig. 4.8-c) assumes that there is a sudden and definite end of the potential core and then immediately the fully developed flow starts. A certain discrepancy in the experimental result is also expected to occur due to the use of the effective diameter as well as due to the inherent inaccuracies associated with the Hydrogen bubble method.

Results on inflow studies have been presented and seem to indicate that the existence of inflow is a function of more than exit Froude number alone.

5.2 Limitations of the Study

One of the main limitations of the study was that it was not possible to obtain the cross section velocity profiles. This is clearly due to the limitations of the Hydrogen bubble measuring system as well as the nature of the buoyant jet.

The lack of these measurements set limitations on the ability to predict the behaviour of the flow in the shear layer as well as the rate of jet expansion. The failure of the LDA to operate satisfactorily deprived the study of the turbulence characteristics of the buoyant jet in the vicinity of the nozzle.

The presence of all the above limitations should indicate that the results obtained in this study will have to be taken with a certain degree of approximation.

5.3 Recommendation for Future Work

The first recommendation for future work would be to attempt to make measurements of the cross section profiles as well as the turbulence measurements. This could be performed by LDA system improvised for this type of flow. A LDA system with forward scatter mode could be experimented with in a set up with large tanks. Some time has to be spent on experimenting with an appropriate seeding material.

The second area of work that requires a serious and extensive study is the problem of inflow. The exact behaviour of inflow and the parameters that trigger it need to be defined more broadly. The effect of the boundary layer needs to be investigated.

References

1. Abraham, G., Jet Diffusion in Liquid of Greater Density, *J. Hydraulic Division, Amer. Soc. Civil Eng.*, 86(HY6), 1-13, 1960.

2. Abraham, G., Jet Diffusion in Stagnant Ambient Fluid, Rep. 29,*Delft Hydraulics Lab., Delft, Netherlands*,1963.

3. Brooks, N. H., Conceptual Design of Submarine Outfalls II. Hydraulic Design of Diffusers, *Tech. Memo 70-2, California Institute of Technology, M. W. Keck Lab of Hyd. and Water Resources*, Jan., 1970.

4. Charlton, J. A., Hydraulic Modelling of Saline Intrusion Into Sea Outfalls, *Proceedings, International Conference on the Hydraulic Modelling of Civil Engineering Structures*, Coventry, England, Sept. 1982, pp 349-356.

5. Chen, C. J., C. P. Nikitopoulos, On the Near Field Characteristics of Axisymmetric Turbulent Jets in a Uniform Environment,*Int. J. of Heat and Mass Transfer*, vol.22, pp 245-255,1979.

6. Chen, C. J., E. Rodi, A Mathematical Model for Stratified Turbulent Flow and its Application to Buoyant Jets, *16th IAHR Congress, Section C.a*, San Paulo, Brazil 1975.

7. Clutter D. W., A. M. O. Smith and J. G. Brazier, Techniques of Flow Visualisation Using Water as the Working Medium, *Douglas Aircraft Company*, Report No. ES29075, April, 1959.

8. Freymuth, P., On Transition in a Separated Laminar Boundary Layer, *J. Fluid Mech.*, 1966, 25, 683-704.

9. George, W. K.,R. L. Alpert, F. Tamanini, Turbulence Measurements in an Axi-symmetric Buoyant Plume, *Int. J. Heat Mass Transfer*, 20, 1145-1154., 1977.

10. Hirst, E., Zone of Flow Establishment for Round Buoyant Jets, *Water Resources Research*, vol. 8, No. 5, 1234-1246. 1972

11. Jörg, O. & R. S. Scorer, An Experimental Study of Cold Inflow into Chimneys, *Atmospheric Environment*, vol. 1, 1967, pp 645-654.

12. Kotsovinos, N. E., Plane Turbulent Buoyant Jets, Part 2, *J. Fluid Mechanics*, vol. 8, 1977, pp 60-61.

13. Morton, B. R., Taylor, G. I. and Turner, J. S., Turbulent Gravitational Convection from Maintained and Instantaneous Sources, *Proc. Roy. Soc.*, London, vol. 234A, 1956, pp 1-23.

14. Morton, B. R., Forced Plumes, *J. of Fluid Mech.*, vol. 5, 1959, pp. 151-163.

15. Nakagome, H. and M. Hirata, The Structure of Turbulent Diffusion in an Axisymmetric Thermal Plume, *Proceedings of the International Centre of Heat and Mass Transfer, Seminar on Turbulent Buoyant Convection*, Dubrovnik,Yugoslavia, pp 365-372. 1976.

16. Pande, B. B. L., A Theoretical and Experimental Study of Heated Surface Discharges into Quiescent Ambients, *Ph D Thesis Civil Engineering, University of Alberta*, 1975.

17. Priestley, C. H. B.,F. K. Ball, Continuous Convection From an Isolated Source of Heat, *Quart. J. Roy. Met. Soc.*, 81(348), 144-157, 1955.

18. Rajaratnam, N., Turbulent Jets,*Elsevier Scientific Publications* , Netherlands, 1976.

19. Rajaratnam, N., Turbulent Plumes and Buoyant jets, *Lecture Notes, Dept. of Civil Engineering, Univ. of Alberta*, Edmonton, Canada, 1984.

20. Rodi, W., (Ed.), Turbulent Buoyant Jets and Plumes, *The Science and applications of Heat and Mass Transfer, Pergamon Press*, 1982.

21. Rouse, H., Yih, C. S. and Humphries, H. W., Gravitational Convection from a Boundary Source, *Tellus*, vol. 4, 1952, pp 201-210.

22. Sami, S., T. Carmody & H. Rouse, Jet Diffusion in the Region of Flow Establishment, *J. of Fluid Mechanics*, 27(2), 231-252, 1966.

23. Steffler P. M., N. Rajaratnam, A. W. Peterson, LDA Measurements in Open Channel, *Hydraulics Division, ASCE*, vol 111, No. 1, Jan. 1985.

24. Taylor, G. I., Flow Induced by Jets, *J. Aerosp. Sci.*, 25, 464-465, 1958.

25. Wilkinson, David L., Purging of Saline Wedges from Ocean Outfalls, *Journal of Hydraulic Engineering, vol. 110, No. 12, ASCE*, Dec. 1984. 1815-1829.

6. APPENDIX A

6.1 Flow Development Region of a Plane Turbulent Buoyant Jet

6.1.1 Introduction

The analysis presented earlier for the axisymmetric turbulent buoyant jet can be extended for the case of a plane buoyant jet. Consider a plane turbulent plume or a buoyant jet rising vertically from a long slot of width $2b_o$ with an almost uniform velocity of U_o with a mass density of ρ_o which is only slightly less than the density ρ_a of the ambient fluid. The centre line velocity of this Boussinesq plume increases continuously with an outer turbulent shear layer penetrating from both sides. At a distance L from the nozzle the turbulent shear layer completely penetrates the plume and establishes a fully developed flow. Starting from this point the centreline velocity decays. Depending on whether the flow at the nozzle is momentum dominated or completely buoyancy dominated its term ranges from jet to plume. The interest here is to present an analysis applicable to both the cases.

6.1.2 Analysis

The continuity equation for a buoyant jet can be approximately written as

$$\frac{\partial u}{\partial x} + \frac{\partial v}{\partial y} = 0 \qquad [6.45]$$

Using the same notation but replacing r by y the momentum equation can be reduced to:

$$u \frac{\partial u}{\partial x} + v \frac{\partial u}{\partial y} = \frac{1}{\rho} \frac{\partial \tau}{\partial y} + \frac{g\Delta\rho}{\rho_o} \qquad [6.46]$$

Here slender flow approximations similar to that in boundary layer analysis, as well as Boussinesq approximation have been made. In Eq. 6.46, g is the acceleration due to gravity, $\Delta\rho$ is the difference between the ambient density ρ_a and the local density ρ, τ is the turbulent shear stress. The laminar shear stress has been assumed to be negligible (Rajaratnam, 1984). The conservation equation for density deficiency can be reduced to:

$$\frac{\partial (u\Delta\rho)}{\partial x} + \frac{\partial (v\Delta\rho)}{\partial y} = \epsilon \frac{\partial^2 \Delta\rho}{\partial y^2} \qquad [6.47]$$

where ϵ is the eddy diffusivity coefficient, asssumed to be constant across the plume at any cross section.

6.1.2.1 Potential Core

Inside the potential core of the rising plume or buoyant jet, assuming negligible turbulence Eq. 6.46 reduces to:

$$u \frac{\partial u}{\partial x} + v \frac{\partial u}{\partial y} = \frac{g\Delta\rho}{\rho_a} \qquad [6.48]$$

On the axis of the jet since v=0 , Eq. 6.48 reduces to

$$u \frac{\partial u}{\partial x} = \frac{g\Delta\rho}{\rho_a} \qquad [6.49]$$

If u_m is the value of u on the axis of the jet at any distance x from the nozzle,

$$\frac{d}{dx} \left(\frac{u_m^2}{2}\right) = \frac{g\Delta\rho_o}{\rho_a} \qquad [6.50]$$

where $\Delta\rho_o = \rho_a - \rho_o$.

On integrating Eq. 6.50,

$$u_m^2 = U_o^2 + 2g \frac{\Delta\rho_o}{\rho_a} x \qquad [6.51]$$

Eq. 6.51 can be written as:

$$\left(\frac{u_m}{U_o}\right)^2 = 1 + \frac{2\ x/b_o}{F_o^2} \qquad [6.52]$$

where $F_o = \dfrac{U_o}{\sqrt{g\ (\Delta\rho_o/\rho_a)\ b_o}}$

b_o being the half slot width of the nozzle.

At the end of the potential core, if U_m is the value of u_m, from Eq. 6.52

$$\left(\frac{U_m}{U_o}\right)^2 = 1 + \frac{2\ L/b_o}{F_o^2} \qquad [6.53]$$

The length of the potential core L will depend upon the built-in acceleration due to the buoyancy as well as the internal penetration of the turbulent shear layer from outside.

For a given F_o, U_m/U_o can be determined if the length of the potential core L is known. In the past, it has been generally assumed that the length of the potential core for plumes and buoyant jets is approximately the same as that of non-buoyant jets. For non-buoyant plane jets, L is about $12b_o$ (Rajaratnam, 1976). But recent observations in this study on circular buoyant jets indicate that L is much smaller than that for the non-buoyant circular jets and is dependent on the initial buoyancy.

For plane turbulent plumes the following relation (Rajaratnam, 1984) can be written in the fully developed region

$$\frac{U_m}{U_o} = \frac{1.297}{a_e^{1/3} F_o^{2/3}} \qquad [6.54]$$

Using $a_e = 0.0136$ Eq. 6.54 can be simplified to

$$\frac{U_m}{U_o} = \frac{2.76}{F_o^{2/3}} \qquad [6.55]$$

On equating Eq. 6.53 and Eq. 6.55 for the point at the end of the potential core

$$1 + \frac{2\ L/b_o}{F_o^2} = \frac{2.76^2}{F_o^{4/3}} \qquad [6.56]$$

simplifying this further

$$\frac{L}{b_o} = (3.78\ F_o^{2/3} - 0.5\ F_o^2) \qquad [6.57]$$

The above equation gives at least an indication that the

length of the potential core for a plume is much smaller than for a jet.

For buoyant jets in the fully turbulent region the following expression based on the concept of varying entrainment coefficient can be written as (Rajaratnam, 1984)

$$\frac{u_m}{U_o} = \left[\frac{21.2}{F_o^2} + \frac{50.7}{(x/b_o)^{3/2}} \right]^{1/3} \qquad [6.58]$$

Equating this expression with the expression for the potential core

$$1 + \frac{2\ (L/b_o)}{F_o^2} = \left[\frac{21.2}{F_o^2} + \frac{50.7}{(L/b_o)^{3/2}} \right]^{2/3} \qquad [6.59]$$

The solution of this equation has been plotted in the figure 6.1.

Figure 6.1 Fo vs Length of the Potential Core for a Plane Plume

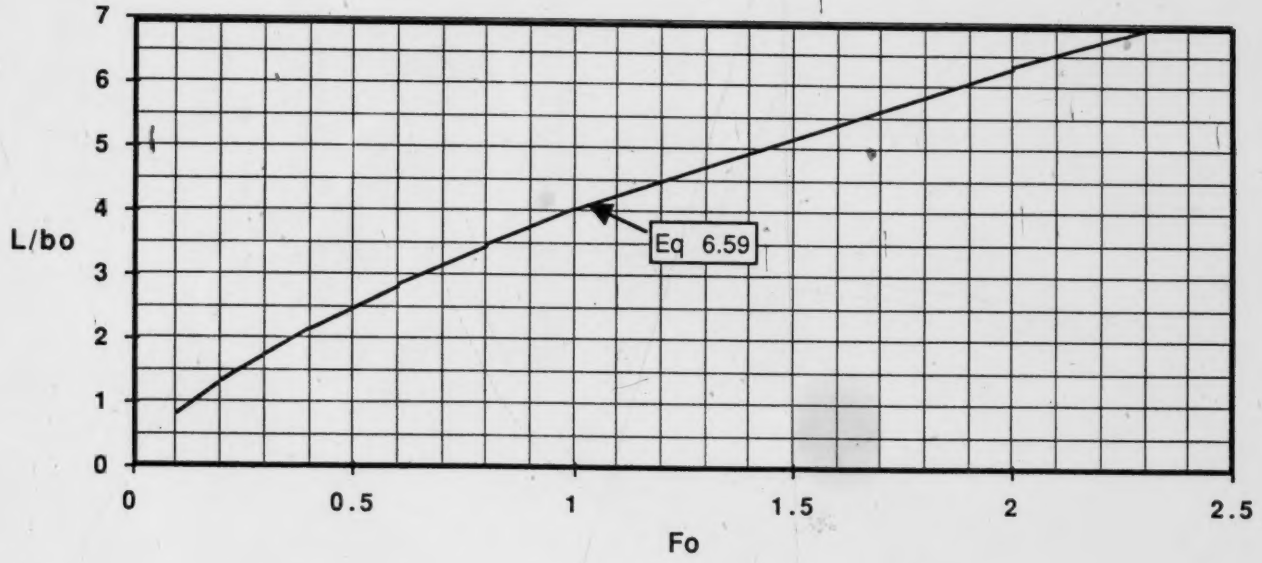

7. APPENDIX B

Figure 7.1 (a-y) Graphical Estimation of the Nozzle Velocity (cm/s)

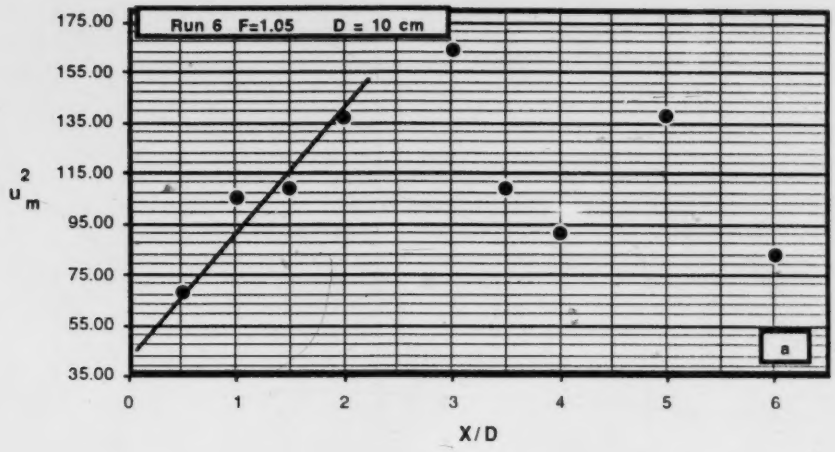

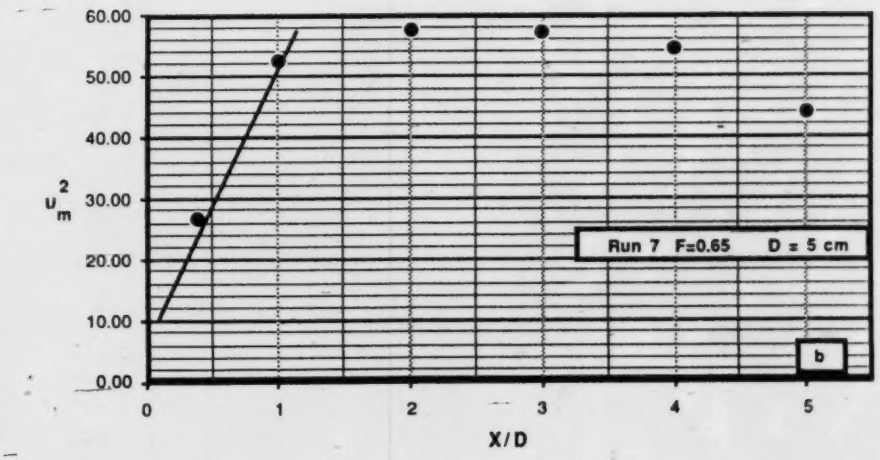

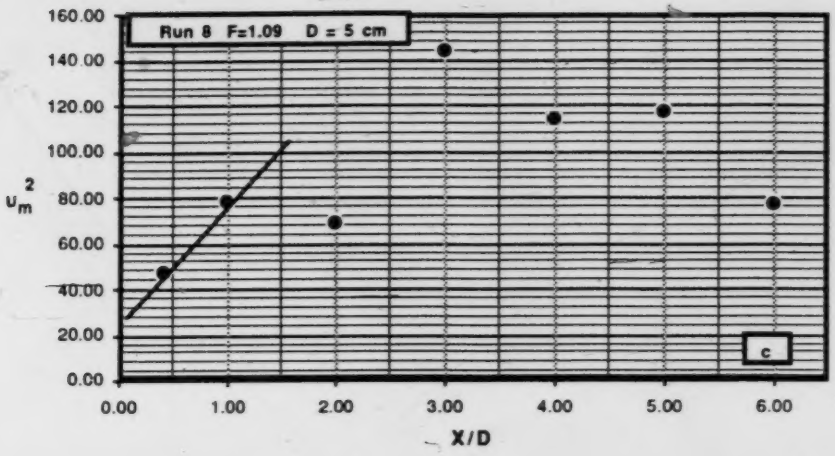
Run 8 F=1.09 D = 5 cm
160.00
140.00
120.00
100.00
80.00
60.00
40.00
20.00
0.00
u_m^2
0.00
1.00
2.00
3.00
4.00
5.00
6.00
X/D
c

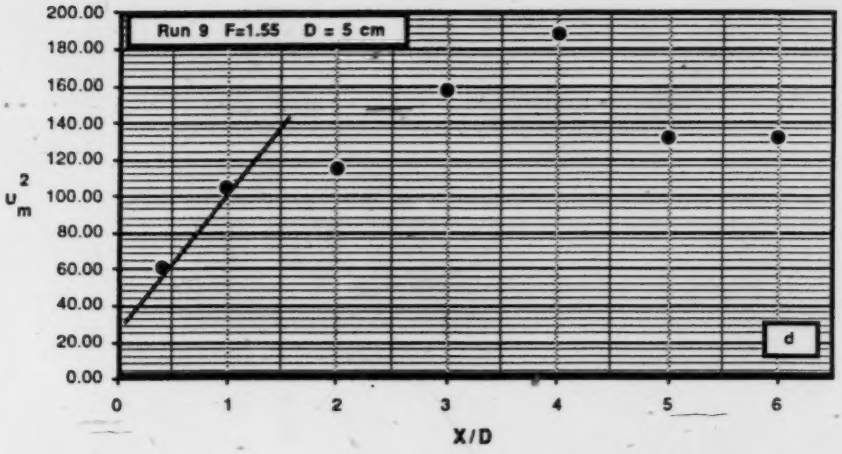
Run 9 F=1.55 D = 5 cm
200.00
180.00
160.00
140.00
120.00
100.00
80.00
60.00
40.00
20.00
0.00
u_m^2
0
1
2
3
4
5
6
X/D
d

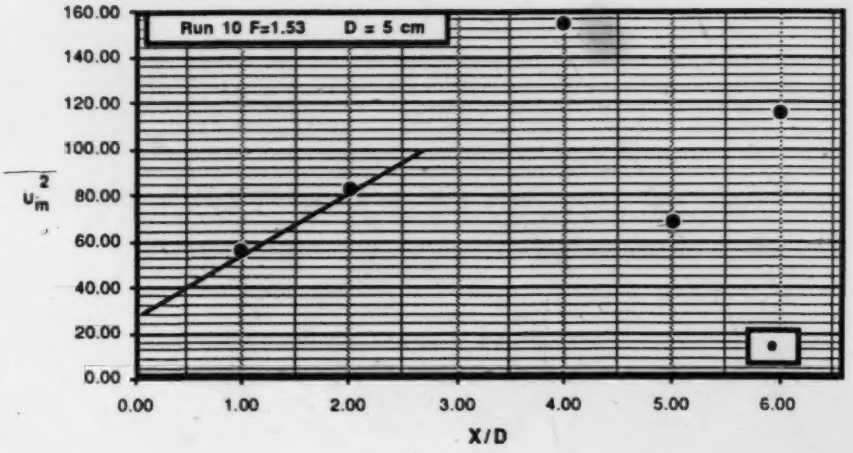
Run 10 F=1.53 D = 5 cm
160.00
140.00
120.00
100.00
80.00
60.00
40.00
20.00
0.00
u_m^2
0.00
1.00
2.00
3.00
4.00
5.00
6.00
X/D

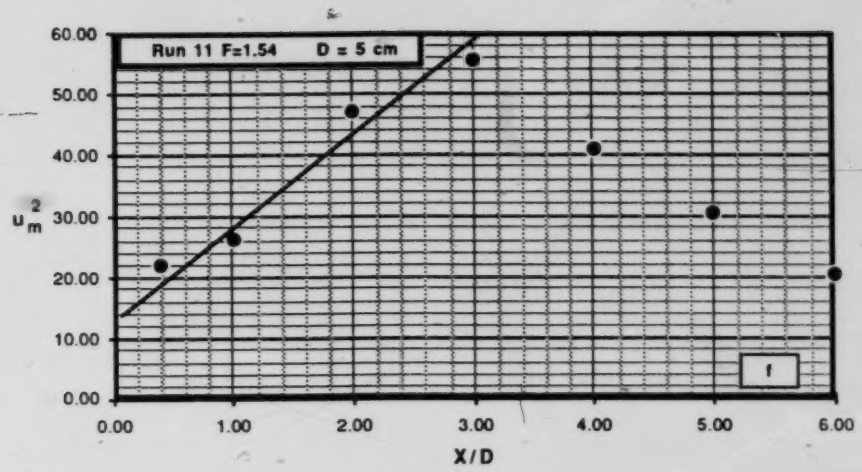
Run 11 F=1.54 D = 5 cm
60.00
50.00
40.00
30.00
20.00
10.00
0.00
u_m^2
0.00
1.00
2.00
3.00
4.00
5.00
6.00
X/D
f

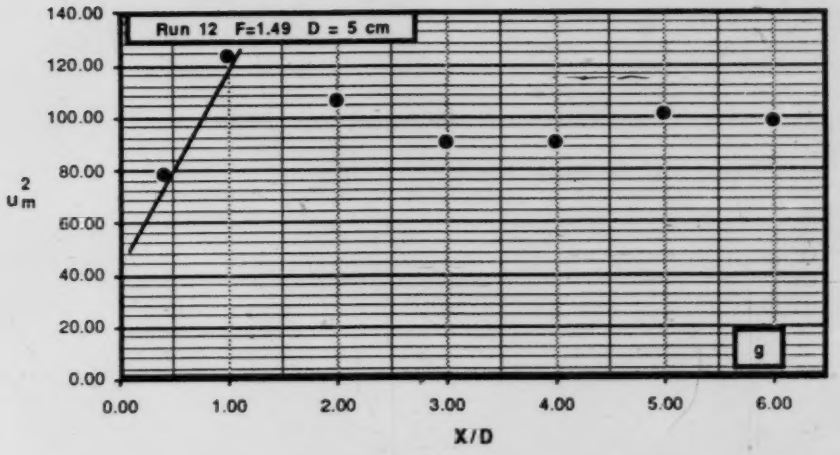
Run 12 F=1.49 D = 5 cm
140.00
120.00
100.00
80.00
60.00
40.00
20.00
0.00
u_m^2
0.00
1.00
2.00
3.00
4.00
5.00
6.00
X/D
g

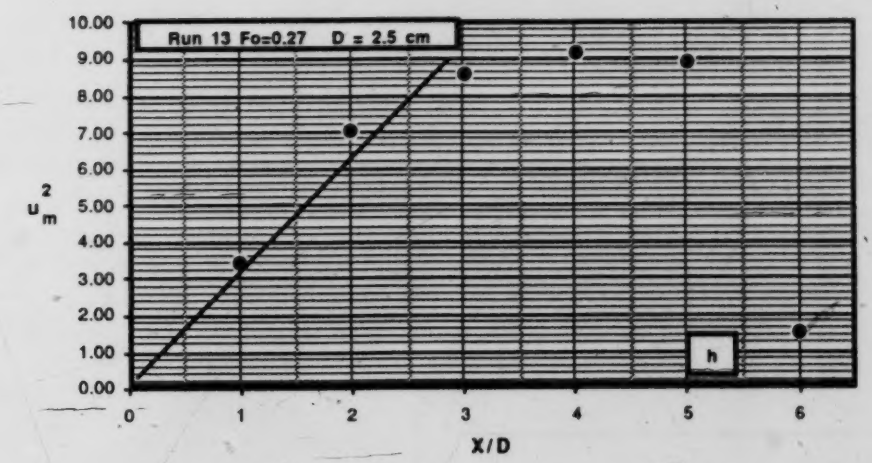
Run 13 Fo=0.27 D = 2.5 cm
10.00
9.00
8.00
7.00
6.00
5.00
4.00
3.00
2.00
1.00
0.00
u_m^2
0
1
2
3
4
5
6
X/D
h

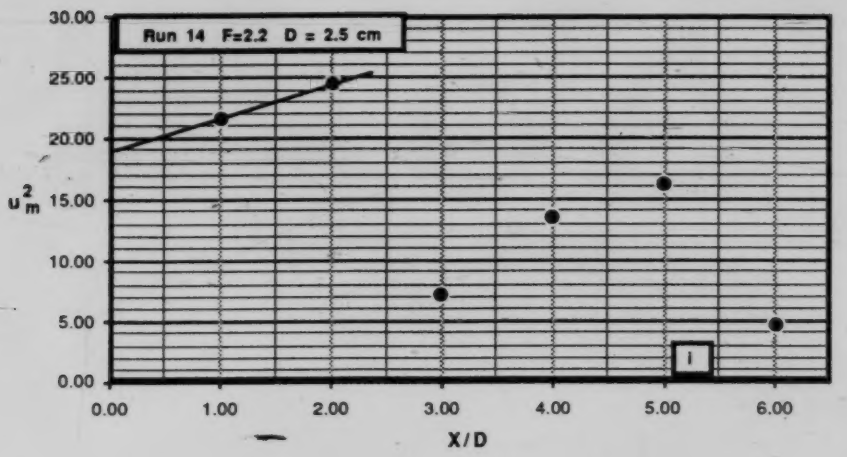
Run 14 F=2.2 D = 2.5 cm
l
u_m^2
X/D
30.00
25.00
20.00
15.00
10.00
5.00
0.00
0.00
1.00
2.00
3.00
4.00
5.00
6.00

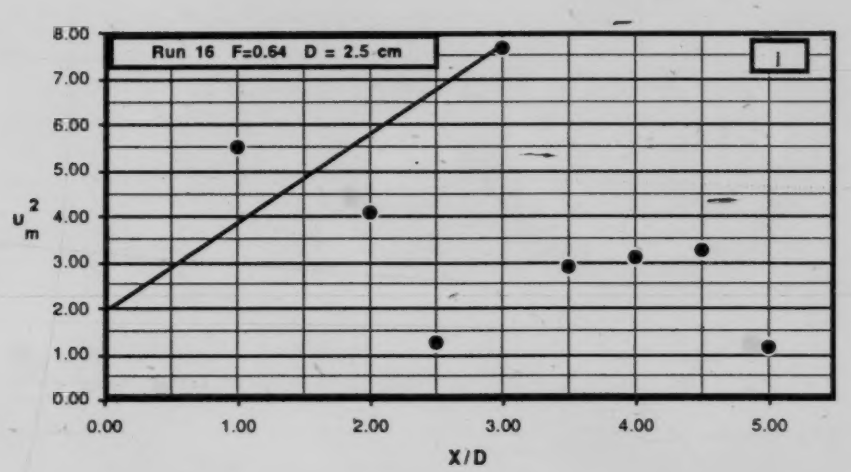
Run 16 F=0.64 D = 2.5 cm
l
u_m^2
X/D
8.00
7.00
6.00
5.00
4.00
3.00
2.00
1.00
0.00
0.00
1.00
2.00
3.00
4.00
5.00

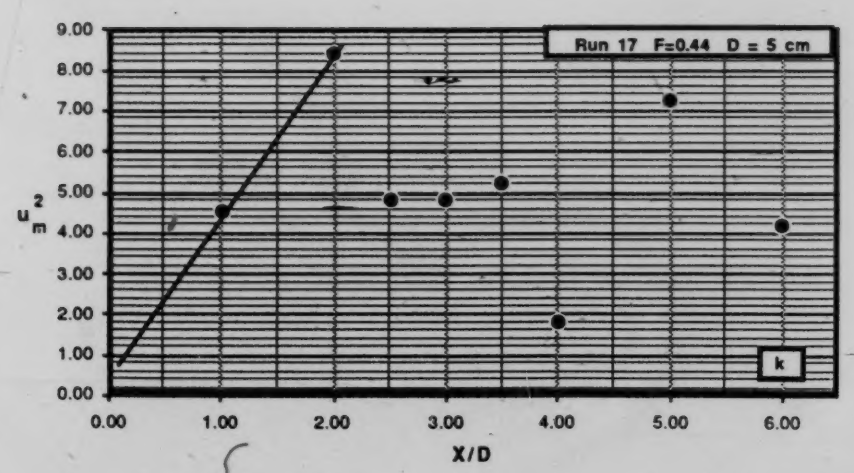
Run 17 F=0.44 D = 5 cm
k
u_m^2
X/D
9.00
8.00
7.00
6.00
5.00
4.00
3.00
2.00
1.00
0.00
0.00
1.00
2.00
3.00
4.00
5.00
6.00

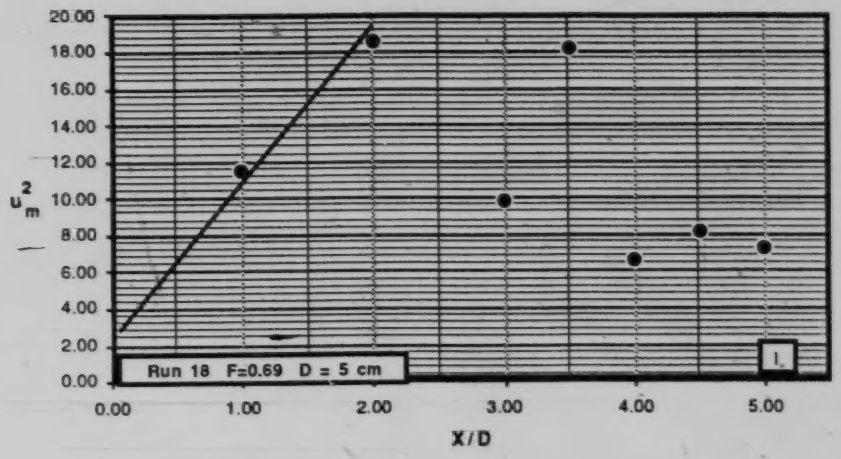
20.00
18.00
16.00
14.00
12.00
10.00
8.00
6.00
4.00
2.00
0.00
u_m^2
Run 18 F=0.69 D = 5 cm
l
0.00
1.00
2.00
3.00
4.00
5.00
X/D

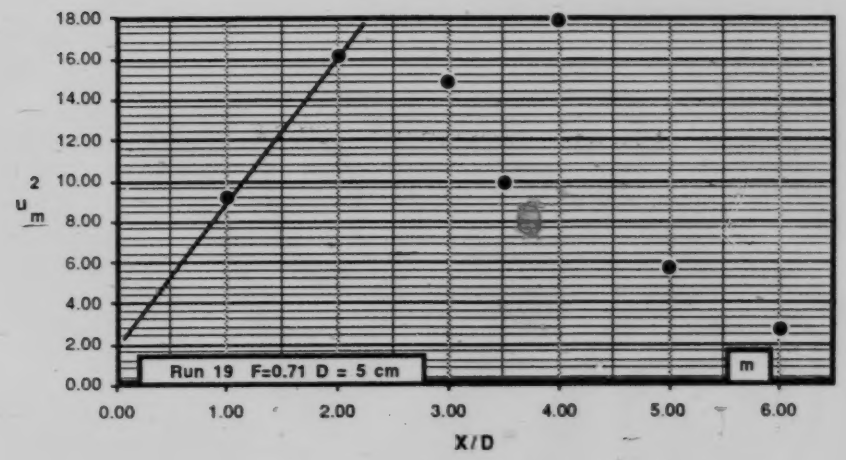
18.00
16.00
14.00
12.00
10.00
8.00
6.00
4.00
2.00
0.00
u_m^2
Run 19 F=0.71 D = 5 cm
m
0.00
1.00
2.00
3.00
4.00
5.00
6.00
X/D

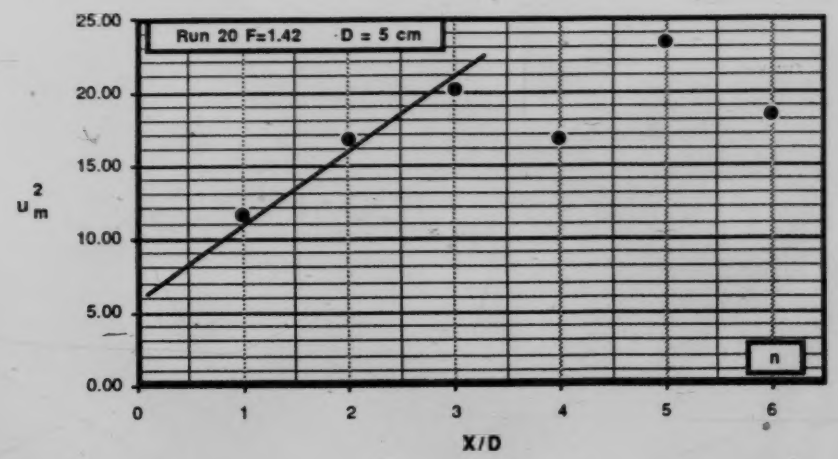
25.00
20.00
15.00
10.00
5.00
0.00
u_m^2
Run 20 F=1.42 D = 5 cm
n
0
1
2
3
4
5
6
X/D

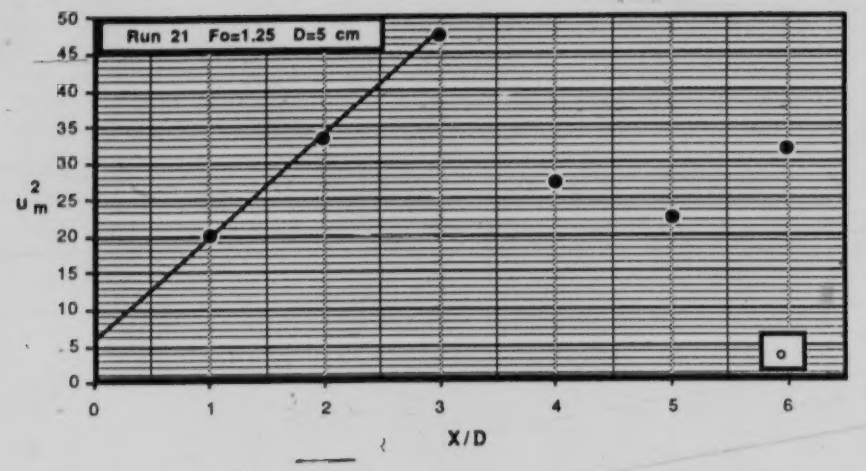
Run 21 Fo=1.25 D=5 cm
o
u_m^2
X/D
0
5
10
15
20
25
30
35
40
45
50
0
1
2
3
4
5
6

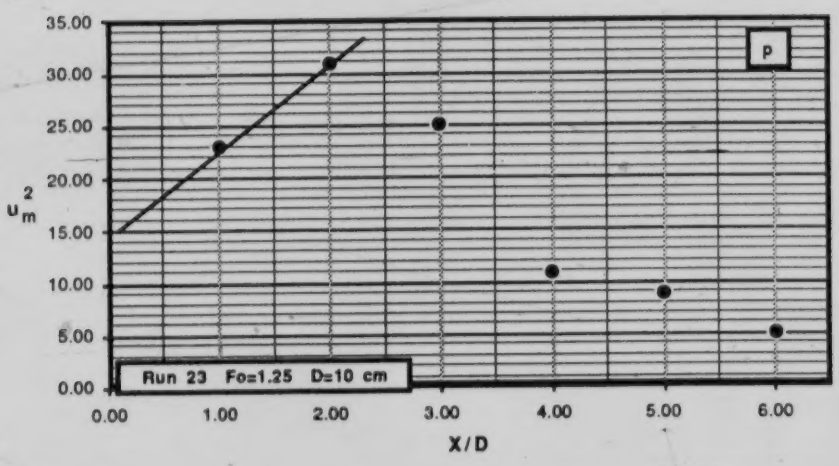
Run 23 Fo=1.25 D=10 cm
p
u_m^2
X/D
0.00
5.00
10.00
15.00
20.00
25.00
30.00
35.00
0.00
1.00
2.00
3.00
4.00
5.00
6.00

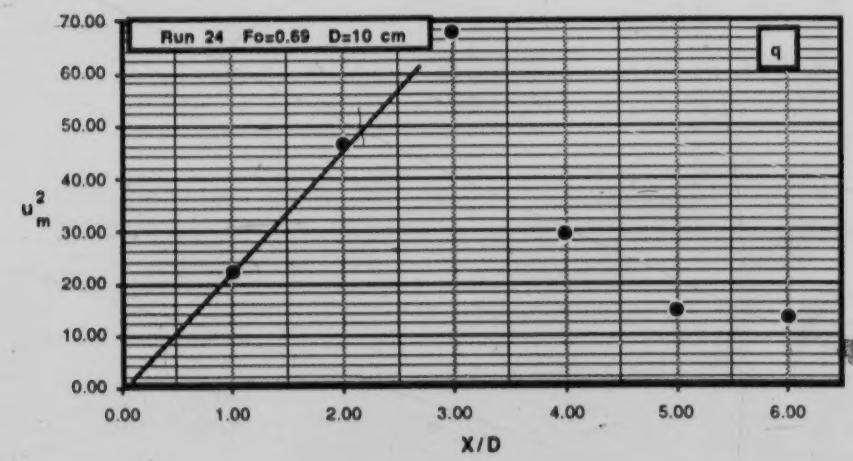
Run 24 Fo=0.69 D=10 cm
q
u_m^2
X/D
0.00
10.00
20.00
30.00
40.00
50.00
60.00
70.00
0.00
1.00
2.00
3.00
4.00
5.00
6.00

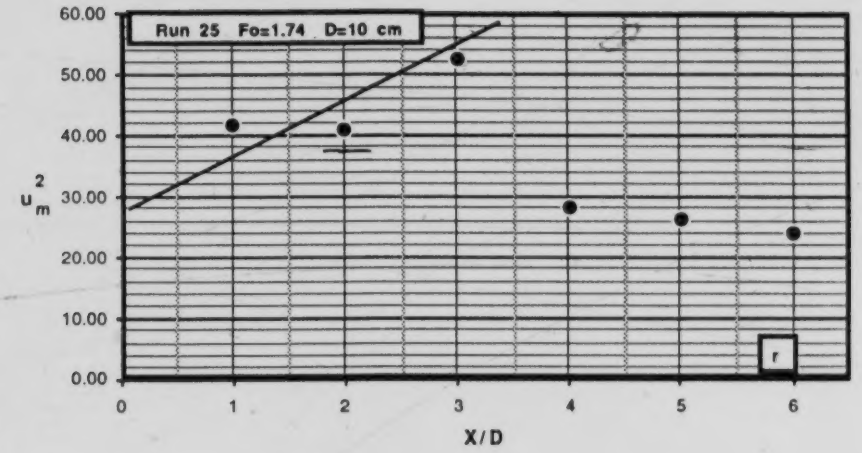
Run 25 Fo=1.74 D=10 cm
60.00
50.00
40.00
30.00
20.00
10.00
0.00
u_m^2
0
1
2
3
4
5
6
X/D
r

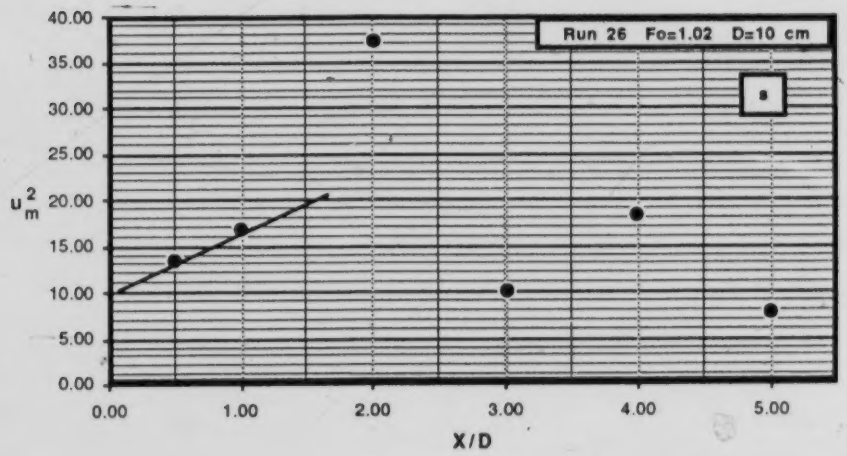
Run 26 Fo=1.02 D=10 cm
40.00
35.00
30.00
25.00
20.00
15.00
10.00
5.00
0.00
u_m^2
0.00
1.00
2.00
3.00
4.00
5.00
X/D
s

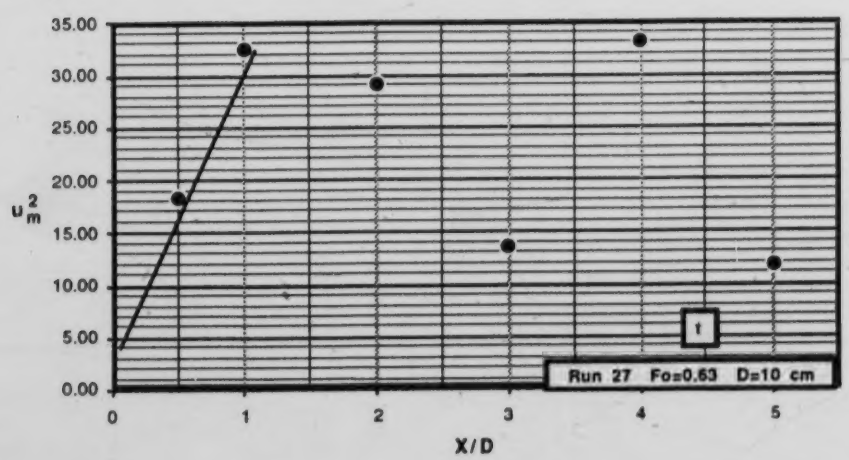
35.00
30.00
25.00
20.00
15.00
10.00
5.00
0.00
u_m^2
0
1
2
3
4
5
X/D
t
Run 27 Fo=0.63 D=10 cm

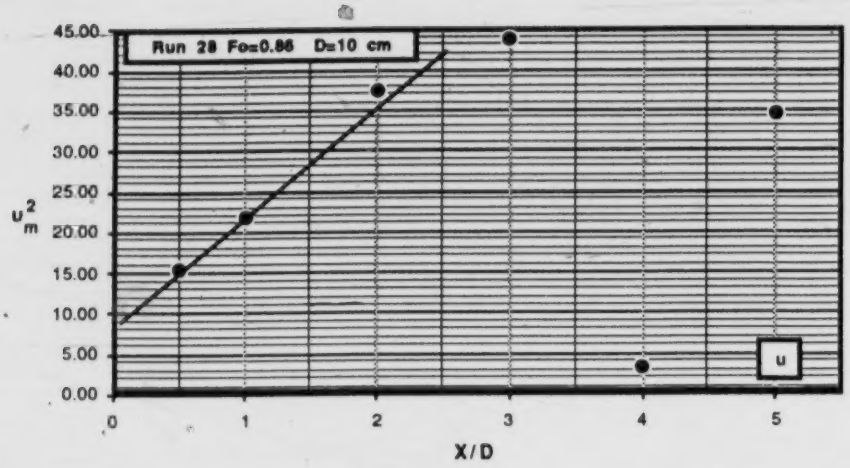
Run 28 Fo=0.86 D=10 cm
45.00
40.00
35.00
30.00
25.00
20.00
15.00
10.00
5.00
0.00
u_m^2
0
1
2
3
4
5
X/D
u

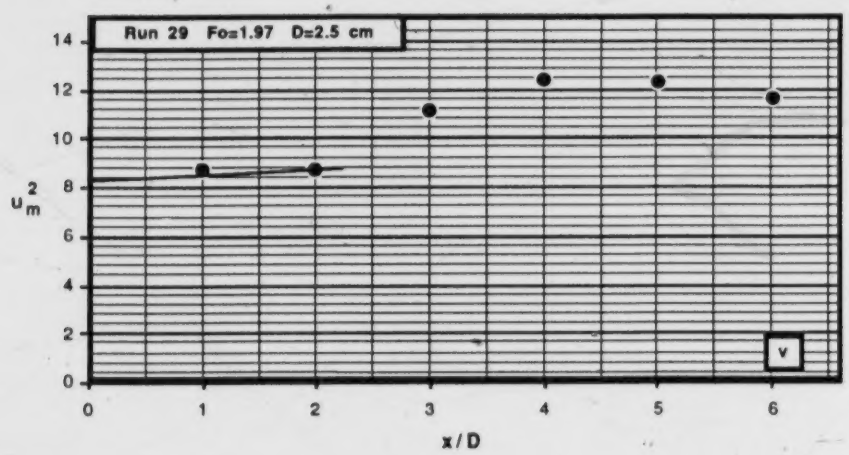
Run 29 Fo=1.97 D=2.5 cm
14
12
10
8
6
4
2
0
u_m^2
0
1
2
3
4
5
6
x/D
v

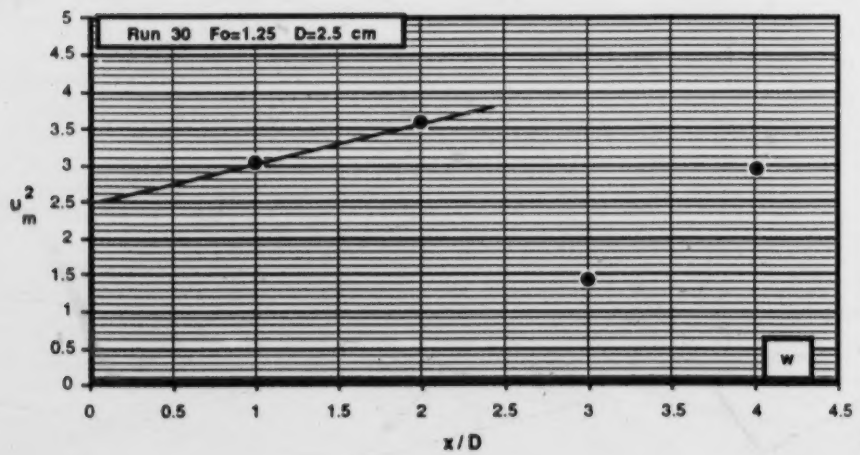
Run 30 Fo=1.25 D=2.5 cm
5
4.5
4
3.5
3
2.5
2
1.5
1
0.5
0
u_m^2
0
0.5
1
1.5
2
2.5
3
3.5
4
4.5
x/D
w

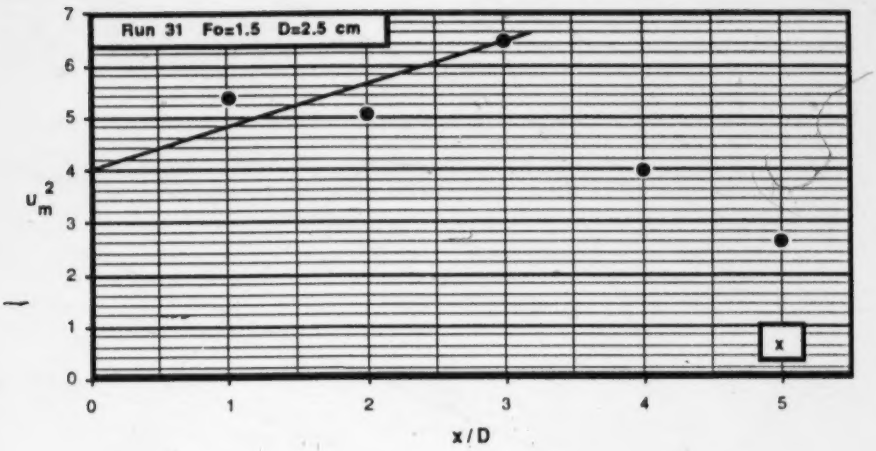
Run 31 Fo=1.5 D=2.5 cm
u_m^2
x/D
x

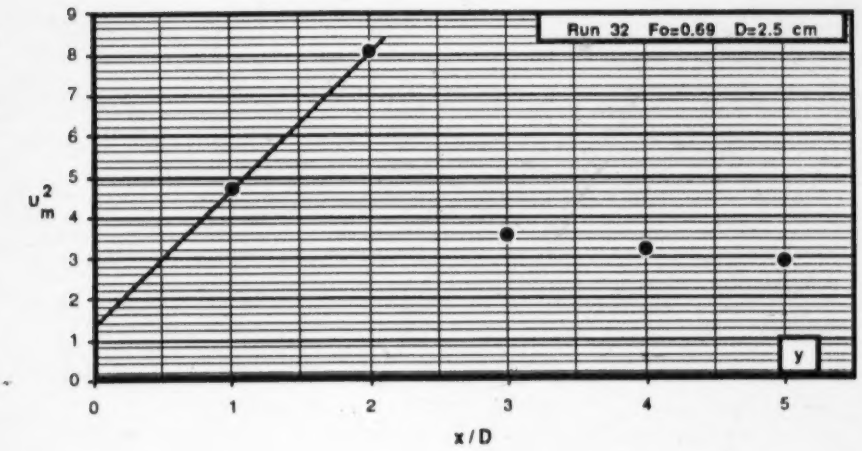
Run 32 Fo=0.69 D=2.5 cm
u_m^2
x/D
y

8. APPENDIX C

Table 8.1 Summary of the Laser Velocity measuremehts

Diameter of the nozzle = 2.5 cm
The velocities are in m/s

		q=1.6gpm	q=10 lpm	q=15 lpm	q=10 lpm
	Q (cms)	0.0001009	0.000167	0.00025	0.000167
	Tp(C)	20.29	21.08	22.78	17.19
	Ta(C)	9.15	8.88	8.61	9.04
	Vo (cm/s)	20.56	33.95	50.93	33.95
	Fo'	10.32	16.08	21.84	21.26
x					
(mm)	x/D				
30	1.2	0.206	0.330	0.518	0.340
75	3	0.222	0.386	0.481	0.325
87.5	3.5	0.268	0.354	0.402	0.345
100	4	0.213	0.396	0.463	0.345
112.5	4.5	0.198	0.338	0.436	0.379
125	5	0.332		0.445	0.269
150	6				0.271

		Q=0.6gpm	q=0.6 gpm	q=15 lpm	q=10lpm
	Q (cms)	0.0000378	0.0000378	0.00025	0.0001667
	Tp	11.67	18.53	19.14	18.40
	Ta	14.87	10.39	8.46	8.98
	Vo	7.71	7.71	50.93	33.95
	Fo'	7.57	4.54	27.02	19.28
x					
(mm)	Y/D				
30	1.2	0.057	0.095	0.500	0.359
50	2	0.060	0.136	0.533	0.396
75	3	0.056	0.130	0.508	0.361
87.5	3.5		0.141	0.495	0.550
100	4		0.132	0.533	0.392
112.5	4.5		0.129	0.480	0.297
125	5				

Figure 8.1 (a-b) u_m/U_o vs x/D for a Buoyant Jet for 2.5 cm Nozzle